DESY-17-155
KEK Preprint 2017-31
LAL 17-059
SLAC–PUB–17161
October 2017

Physics Case for the 250 GeV Stage of the International Linear Collider

LCC Physics Working Group

Keisuke Fujii[1], Christophe Grojean[2,3], Michael E. Peskin[4] (Conveners); Tim Barklow[4], Yuanning Gao[5], Shinya Kanemura[6], Hyungdo Kim[7], Jenny List[2], Mihoko Nojiri[1,8], Maxim Perelstein[9], Roman Pöschl[10], Jürgen Reuter[2], Frank Simon[11], Tomohiko Tanabe[12], James D. Wells[13], Jaehoon Yu[14]; Mikael Berggren[2], Moritz Habermehl[2], Sunghoon Jung[7], Robert Karl[2], Tomohisa Ogawa[1], Junping Tian[12]; James Brau[15], Hitoshi Murayama[8,16,17] (ex officio)

ABSTRACT

The International Linear Collider is now proposed with a staged machine design, with the first stage at 250 GeV with a luminosity goal of 2 ab^{-1}. In this paper, we review the physics expectations for this machine. These include precision measurements of Higgs boson couplings, searches for exotic Higgs decays, other searches for particles that decay with zero or small visible energy, and measurements of e^+e^- annihilation to W^+W^- and 2-fermion states with improved sensitivity. A summary table gives projections for the achievable levels of precision based on the latest full simulation studies.

[1] High Energy Accelerator Research Organization (KEK), Tsukuba, Ibaraki, JAPAN
[2] DESY, Notkestrasse 85, 22607 Hamburg, GERMANY
[3] Institut für Physik, Humboldt-Universität zu Berlin, 12489 Berlin, GERMANY
[4] SLAC, Stanford University, Menlo Park, CA 94025, USA
[5] Center for High Energy Physics, Tsinghua University, Beijing, CHINA
[6] Department of Physics, Osaka University, Machikaneyama, Toyonaka, Osaka 560-0043, JAPAN
[7] Dept. of Physics and Astronomy, Seoul National Univ., Seoul 08826, KOREA
[8] Kavli Institute for the Physics and Mathematics of the Universe, University of Tokyo, Kashiwa 277-8583, JAPAN
[9] Laboratory for Elementary Particle Physics, Cornell University, Ithaca, NY 14853, USA
[10] LAL, Centre Scientifique d'Orsay, Université Paris-Sud, F-91898 Orsay CEDEX, FRANCE
[11] Max-Planck-Institut für Physik, Föhringer Ring 6, 80805 Munich, GERMANY
[12] ICEPP, University of Tokyo, Hongo, Bunkyo-ku, Tokyo, 113-0033, JAPAN
[13] Michigan Center for Theoretical Physics, University of Michigan, Ann Arbor, MI 48109, USA
[14] Department of Physics, University of Texas, Arlington, TX 76019, USA
[15] Center for High Energy Physics, University of Oregon, Eugene, Oregon 97403-1274, USA
[16] Department of Physics, University of California, Berkeley, CA 94720, USA
[17] Theoretical Physics Group, Lawrence Berkeley National Laboratory, Berkeley, CA 94720, USA

Contents

1 Introduction

The International Linear Collider (ILC) is a linear electron-positron collider planned for physics exploration and precision measurements in the energy region of 200–500 GeV. This report summarizes the expectations for measurements of the Higgs boson and searches for physics beyond the Standard Model in the program of this accelerator at 250 GeV in the center of mass.

The physics potential of the ILC is known to be very impressive. A detailed accounting of the expectations for this machine was presented in 2013 as a part of the ILC Technical Design Report [1, 2] and in white papers prepared for the American Physical Society's study of the future of US particle physics (Snowmass 2013) [3–6]. As the ILC experiments have been studied in more detail, our Working Group has published updated expectations for the general ILC program [7] and for the direct search for new particles at this collider [8].

In the past year, the program of the ILC has been reshaped in the expectation of an international agreement and start of construction. The Linear Collider Collaboration has recast the project as a staged program with the first stage at 250 GeV [9]. This would significantly lower the initial cost of the machine and provide a focused, nearer-term goal for the project. In this approach, the 250 GeV stage of the ILC needs to be justified on its own merit rather than as a part of a broader program that includes running at higher energies. At the same time, new studies have revealed a very strong physics potential for the 250 GeV stage of the ILC that was not specifically emphasized in the reports cited above. The purpose of this article is to summarize the case for the 250 GeV machine stage as it is understood today. We will see that there is a compelling physics case for the ILC that applies already at its 250 GeV stage.

Section 2 of this report updates the 2015 report on ILC operating scenarios [10], giving estimates of time vs. integrated luminosity for an ILC project with 250 GeV, top quark threshold, and 500 GeV stages.

The most important objective of a 250 GeV e^+e^- collider is to make precision measurements of the couplings of the 125 GeV Higgs boson to vector bosons, quarks, and leptons. Unlike the situation at proton colliders, all of the major Standard Model decay modes of the Higgs boson will be individually identifiable in e^+e^- experiments. This means that it is possible to extract the absolute strengths of Higgs boson couplings to high precision in a model-independent analysis. In Sections 3 and 4 of this report, we will explain how this can be done and give projected errors for the coupling constant determinations.

The search for new physics beyond the Standard Model is probably the most important goal of particle physics today. The LHC experiments are carrying out

intensive searches for new particle of many types, and dark matter detection experiments add to the variety of searches. Because shifts of the Higgs couplings can be induced by mixing with or loop corrections from very heavy particles, the study of these couplings gives a route to new physics that is essentially orthogonal to these methods. Today, the LHC experiments are probing for large shifts of the Higgs couplings, but, in typical models, the shifts of the Higgs couplings from their Standard Model values are predicted to be small, at the 10% level and below. Thus, high-precision experiments, beyond the expectations for LHC, are needed. *In our opinion, this precision study of the Higgs boson is the most important suggested probe for new physics beyond the Standard Model that is not currently being exploited.* This gives special impetus to the construction of a new accelerator for precision Higgs studies.

Qualitatively different models of new physics predict different patterns of deviation from the Standard Model prediction. If the Higgs couplings can be measured individually with high precision, it is possible to read the pattern and obtain information on the properties of the new physics model. We will expand on this point and present some examples in Section 5.

The Higgs boson provides another possible window into new physics. Potentially, it is easy for the Higgs boson to couple to new particles with no Standard Model interactions, particles that might make up the dark matter or might otherwise be hidden from experiments that rely on other probes. We will review the ILC capabilities for the discovery of invisible and exotic Higgs decays in Section 6.

In Sections 7, 8, and 9, we will discuss the capabilities of a 250 GeV e^+e^- collider beyond its program on the Higgs boson. Section 7 will review the reach of such a machine for observation of the direct pair production of dark matter particles and other particles difficult to detect at the LHC. In Section 8, we will discuss the new information that will be available from the precision study of $e^+e^- \to W^+W^-$. In Section 9, we will review the ability of e^+e^- annihilation to fermion-antifermion pairs at 250 GeV to probe for new boson resonances and quark and lepton substructure.

Finally, in Section 10, we will review very briefly the capabilities of the ILC, after an energy upgrade, for measurements at 350 GeV, 500 GeV, and higher energies. Indeed, the infrastructure of the ILC will support a long future of experiments with e^+e^- collisions that would build on the success of the first 250 GeV stage.

An appendix gives a table of the projected measurement errors for the most important parameters. We recommend that these are the numbers that should be used in discussions of the ILC physics prospects and in comparisons of the ILC with other proposed facilities.

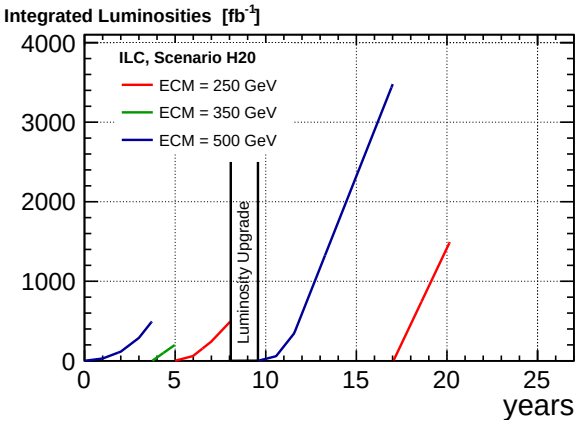

Figure 1: The nominal 20-year running program for the 500-GeV ILC [10].

2 Plan for ILC evolution and staging

Following the publication of the ILC Technical Design Report [1,2,11–13], a canonical operating scenario was defined for the ILC [10]. This operating scenario assumed the construction of a 500-GeV machine, which within a 20-year period would accumulate integrated luminosities of $4\,\mathrm{ab}^{-1}$, $2\,\mathrm{ab}^{-1}$ and $200\,\mathrm{fb}^{-1}$ at center-of-mass energies of 500 GeV, 250 GeV and 350 GeV, respectively, with beam polarizations of $\pm 80\%$ for the electron beam and $\pm 30\%$ for the positron beam. Figure 1 shows the time evolution of the data-taking envisioned in [10], starting with operation at 500 GeV. There were three main physics reasons for starting at 500 GeV: first, the ability to use both of the major Higgs boson production processes $e^+e^- \to Zh$ and $e^+e^- \to \nu\bar{\nu}h$ to measure Higgs couplings; second, the ability to begin precision measurements of the couplings of the top quark, including the direct measurement of the top-Yukawa coupling from $t\bar{t}h$ production, and third, the ability to exploit the maximal discovery range for new particles.

Nevertheless, a very important part of the ILC physics program relies on data collected in its running at 250 GeV, which already yields a substantial sample of about half a million Higgs bosons tagged with recoiling Z bosons and subject to very small backgrounds. Using new analyses for reconstructing the various Higgs decay modes and a new, more powerful theoretical approach, to be described in Section 3, we realized that the 250 GeV program alone can already give powerful and model-independent constraints on the Higgs properties. Thus, a staging scenario with a long first stage at 250 GeV makes sense from the point of view of physics. The purpose of this paper is to present this argument in detail.

The detailed plan and accelerator design for the 250 GeV stage of the ILC is described in [9]. In this section, we will discuss the implications of this plan for the

running scenario and luminosity expectations.

Construction of a 250 GeV machine rather than the full 500 GeV machine does change the expectation for the instantaneous luminosity that can be assumed in 250 GeV running. The original running scenario (Fig. 1) relied on the availability of the full cryogenic and radio-frequency power of the 500-GeV machine in order to double the repetition rate from 5 to 10 Hz when operating at 250 GeV. This option is not available when only half of the power is installed in a minimal 250 GeV machine. Therefore the total operating time for accumulating the same integrated luminosities as listed above stretches to 15 years of operation for the 250 GeV stage and to 26 years for the full ILC program. This luminosity evolution is shown in Fig. 2a.

There is a cost-neutral possibility to increase the instantaneous luminosity by focussing the beam more strongly at the IP. This increases the level of beamstrahlung and e^+e^- pair production. However, the ILC interaction region is designed to cope with operation at 500 GeV and even at 1 TeV. Since beamstrahlung is strongly energy-dependent, its effects at energies lower than these is much reduced, and so there is room for a more aggressive choice of beam parameters at 250 GeV. A revised set of accelerator parameters that implements this luminosity enhancement is presented in Section 5 of [9]. The effect of these new parameters on the run plan is illustrated in Fig. 2b. In this plan, the length of the 250 GeV stage is 11 years and the total operating time for the full program is only slightly longer than the original 20 years. The exact effects of the new beam parameters on the detectors and the physics measurements, taking account of the new beam energy spectrum and pair background, still need to be evaluated quantitatively. All physics studies quoted in this document are performed with the TDR parameters and thus apply strictly speaking to the case shown in Fig. 2a. Nevertheless, we expect the differences to be small and are optimistic that similar results will be found with the new beam parameters corresponding to Fig. 2b.

It is well documented that beam polarization plays an essential role in the physics program of the ILC at higher energies [2]. The importance of having both electron and positron beam polarization at 250 GeV, for Higgs measurements and for other aspects of the ILC physics program, is discussed in some detail in [14]. Thus, in accord with the machine specifications presented in [9], we assume beam polarizations of 80% and 30% for the electron and positron beams of the 250 GeV ILC. In [10], the fractions of integrated luminosity dedicated to each of the four possible sign combinations were proposed for each center-of-mass energy. For operation at 250 GeV, fractions of (67.5%, 22.5%, 5%, 5%) were forseen for ($-+$,$+-$,$--$,$++$), where the first sign applies to the electron beam polarization and the second to that of the positron beam, giving emphasis to the $-+$ configuration as it has the largest Higgs production cross section. In our new theory framework, the left-right cross-section asymmetry plays an important role. To optimize the measurement of this quantity, we assume in this paper a sharing of (45%, 45%, 5%, 5%) among the various beam polarization choices.

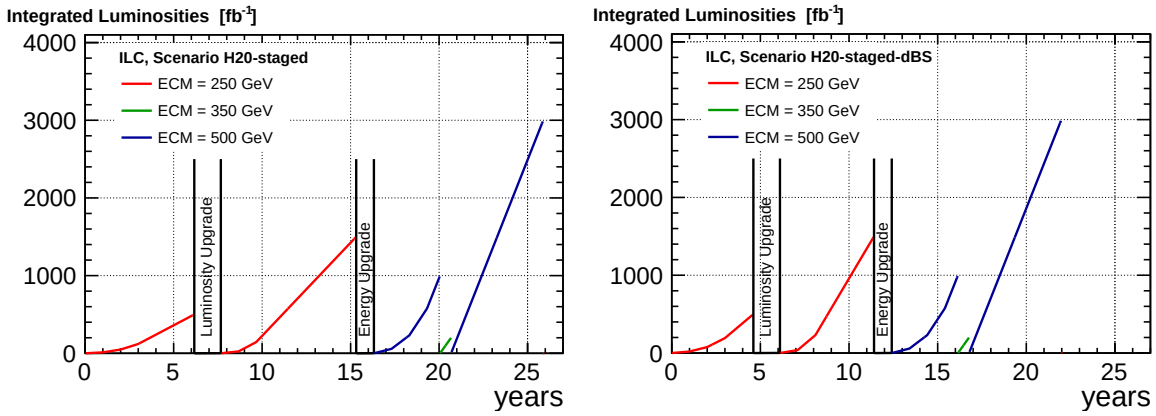

(a) (b)

Figure 2: Run plan for the staged ILC starting with a 250-GeV machine under two different assumptions on the achievable instantaneous luminosity at 250 GeV. Both cases reach the same final integrated luminosities as in Fig. 1.

3 Effective Field Theory approach to precision measurements at e^+e^- colliders

The goal of the ILC program on the Higgs boson is to provide determinations of the various Higgs couplings that are both high-precision and model-independent.

It is easy to see how this can be achieved for some combinations of Higgs couplings. In the reaction $e^+e^- \to Zh$, the Higgs boson is produced in association with a Z boson at a fixed lab-frame energy (110 GeV for $\sqrt{s} = 250$ GeV). Up to small and calculable background from $e^+e^- \to ZZ$ plus radiation, observation of a Z boson at this energy tags the presence of a Higgs boson. Then the total cross section for $e^+e^- \to Zh$ can be measured absolutely without reference to the Higgs boson decay mode, and the various branching ratios of the Higgs boson can be observed directly.

The difficulty comes when one wishes to obtain the absolute strength of each Higgs coupling. The coupling strength of the Higgs boson to $A\overline{A}$ can be obtained from the partial width $\Gamma(h \to A\overline{A})$, which is related to the branching ratio through

$$BR(h \to A\overline{A}) = \Gamma(h \to A\overline{A})/\Gamma_h \ , \tag{1}$$

where Γ_h is the total width of the Higgs boson. In the Standard Model (SM), the width of a 125 GeV Higgs boson is 4.1 MeV, a value too small to be measured directly from reaction kinematics. So the width of the Higgs boson must be determined indirectly, and this requires a model formalism.

In most of the literature on Higgs boson measurements at e^+e^- colliders, the width is determined using the κ parametrization. One assumes that the Higgs coupling to

each species A is modified from the SM value by a mutiplicative factor κ_A. Then, for example,

$$\frac{\Gamma(h \to ZZ^*)}{SM} = \kappa_Z^2 \ , \qquad \frac{\sigma(e^+e^- \to Zh)}{SM} = \kappa_Z^2 \ . \tag{2}$$

where SM denotes the SM prediction. The e^+e^- environment offers a sufficient number of measurements to determine all of the relevant parameters κ_A. In particular, the ratio

$$\sigma(e^+e^- \to Zh)/BR(h \to ZZ^*) \tag{3}$$

is independent of κ_Z and directly yields the Higgs width. However, at the 250 GeV ILC even with 2 ab^{-1} of data, the statistics to measure $BR(h \to ZZ^*)$ is limited, and so the precision of the width determination is compromised. In the earlier literature, including [3, 7], this problem was solved by using data from higher energies, making use of the W fusion reaction and the larger and more precisely measurable branching ratio $BR(h \to WW^*)$.

There is a more serious problem with the κ formalism: It is not actually model-independent. In principle, the Higgs boson can have couplings to ZZ with two different structures,

$$\delta\mathcal{L} = \frac{m_Z^2}{v}(1+\eta_Z)hZ_\mu Z^\mu + \zeta_Z \frac{1}{v} hZ_{\mu\nu}Z^{\mu\nu} \ . \tag{4}$$

Here the coefficients η_Z, ζ_Z represent independent corrections due to new physics effects.* The Higgs boson coupling to WW has a similar structure, with parameters η_W, ζ_W. In the κ formalism, the couplings ζ_Z, ζ_W are assumed to be zero. The operator multiplying ζ_Z is momentum-dependent, so the effect of this term depends on the momentum configuration of the vector bosons. Indeed, for a 125 GeV Higgs boson and $\sqrt{s} = 250$ GeV,

$$\begin{aligned} \Gamma(h \to ZZ^*)/SM &= (1 + 2\eta_Z - 0.50\zeta_Z) \\ \sigma(e^+e^- \to Zh)/SM &= (1 + 2\eta_Z + 5.7\zeta_Z) \ . \end{aligned} \tag{5}$$

Then the Z coupling information does not cancel out of (3) and so this ratio does not determine the Higgs width unambiguously.

There is an attractive solution to this problem. The fact that the LHC experiments have not yet observed new particles due to physics beyond the SM suggests that these particles are heavy, with masses above 500 GeV for electroweakly coupled states and above 1 TeV for strongly interacting states. If indeed new particles are sufficient heavy, we can describe the physics of the 125 GeV Higgs boson by integrating these particles out of the Lagrangian and replacing their effects by an expansion in operators

*In principle, additional structures can be formed by making η_Z and ζ_Z functions of momentum. However, (4) is the most general structure that appears in the SM perturbed by dimension-6 operators only, a restriction that we will make below.

built of Standard Model fields. The SM itself is the most general gauge-invariant Lagrangian built of SM fields with operators of dimension up to 4. Corrections to the SM are then described by the addition of operators of dimension 6 and higher. If the minimum mass of the new particles is M, operators of dimension 6 will have coefficients proportional to m_h^2/M^2. These represent the first order in an expansion in m_h^2/M^2. Possible operators of dimension 8 and higher are multiplied by additional factors of m_h^2/M^2. It is then suggested to parametrize the effects of the most general new physics on the Higgs boson by writing an effective Lagrangian that consists of the SM Lagrangian plus the most general set of $SU(3) \times SU(2) \times U(1)$-invariant dimension-6 operators. This is called the Standard Model Effective Field Theory (EFT) formalism.

The EFT formalism has been accepted by the LHC community as the best way to parametrize deviations from the SM in Higgs physics and in vector boson interactions that might be observed at the LHC [15]. The advantage of this approach for the LHC experiments is that it provides a precise theoretical formalism in which radiative corrections can be computed. This is important at the LHC, because Higgs signatures often require suppressed decay modes with contributions from different basic couplings (for example, dileptons in the final state), and because quantitative predictions for QCD processes require NLO corrections. However, it is difficult to use this formalism in a completely general way at the LHC. The most important difficulty is that the the number of possible dimension 6 operators is very large. There are 59 dimension-6 operators that can be added to the SM Lagrangian even if we restrict ourselves to one generation of fermions and to baryon number-conserving operators. Most of these involve quark and gluon fields and are relevant to LHC reactions.

For reactions that involve only SM vector bosons, Higgs bosons, and light leptons, the number of possible operators is much smaller, though still sizable. In [16], it is argued that the most general effects of high-mass new physics on these reactions can be parametrized by 10 dimension-6 operators.[†] The same 10 operators parametrize the new physics contributions to precision electroweak observables and to observables in $e^+e^- \to W^+W^-$. There are sufficient measurements available to an e^+e^- collider to determine all 10 parameters without significant degeneracies. This gives a unified formalism for testing the SM, one that brings together the full set of measurements available at an e^+e^- collider. Inclusion of on-shell Higgs decays brings in 7 additional operators. Measurement of Higgs decays allows the coefficients of these additional operators to be determined also. Fits to prospective e^+e^- collider data using the EFT formalism have been presented in [17–20]. The last of these papers emphasizes the completeness of the 17-parameter model and the ability to fit the 17 parameters simultaneously using the expected data set from e^+e^- colliders.

[†]Of these 10 operators, 1 shifts the triple- and quadruple-Higgs couplings but does not affect single-Higgs processes at the tree level.

An illustration of the power of this formalism is given by the answer to the question posed at the beginning of this section. The problem, again, is that the hZZ and hWW couplings each involve two separate kinematic structures whose coefficients must be separately determined. The EFT formalism contains coefficients of dimension-6 operators that contribute to the $\eta_{Z,W}$ and $\zeta_{Z,W}$ parameters defined in (4). However, the $SU(2) \times U(1)$-invariance of the EFT Lagrangian leads to relations between the coefficients for Z and W. These relations are not simple, but they turn out to be very constraining. For the η parameters,

$$\begin{aligned} \eta_W &= -\frac{1}{2} c_H + 2\delta m_W - \delta v \\ \eta_Z &= -\frac{1}{2} c_H + 2\delta m_Z - \delta v - c_T \ , \end{aligned} \tag{6}$$

where the c_i are coefficients of dimension-6 operators, δm_W, δv, and δm_Z are combinations of these coefficients that shift the parameters m_W, G_F, and m_Z (and are constrained by the measured values of those quantities), and c_T is essentially the T parameter of precision electroweak formalism [21] and is constrained to be small by precision electroweak measurements. Similarly,

$$\begin{aligned} \zeta_W &= (8 c_{WW}) \\ \zeta_Z &= \cos^2\theta_w (8 c_{WW}) + 2 \sin^2\theta_w (8 c_{WB}) + (\sin^4\theta_w / \cos^2\theta_w)(8 c_{BB}), \end{aligned} \tag{7}$$

in which the parameters c_{WB}, c_{BB} also contribute to $e^+e^- \to W^+W^-$ and the Higgs decays to $\gamma\gamma$ and $Z\gamma$ and so can be strongly constrained. The network of constraints essentially reduces the problem to be solved by ILC Higgs measurements to the determination of the two parameters c_H, c_{WW} using measurements of the process $e^+e^- \to Zh$ and the decay $h \to WW^*$. For both reactions, there will be ample statistics at the 250 GeV ILC. A particular feature of interest is that new Higgs observables not previously considered in ILC studies become relevant. In particular, the polarization asymmetry and angular distributions in $e^+e^- \to Zh$ turn out to put very strong constraints on ζ_Z or c_{WW} [20].

Remarkably, then, the EFT formalism, applied to the e^+e^- world, realizes in a very beautiful way the hopes put forward by its proponents in the LHC world. It provides a single formalism that knits together constraints from precision electroweak measurements and from all of the processes, not only Higgs processes, that are measured in high-energy e^+e^- reactions. The number of free parameters, describing the most general new physics perturbation, is large but manageable, and all relevant parameters can be determined independently. Although second-order electroweak corrections to already small perturbations are not obviously relevant, the formalism also provides a Lagrangian setting in which radiative corrections can be computed unambiguously. This formalism thus provides a powerful method for stringent tests of the SM and, we hope, discovery of new, beyond-SM effects.

4 Measurement of Higgs boson couplings

In the SM, all of the Higgs boson couplings are predicted in terms of the value of the mass of Higgs boson, which is now known to 0.2% accuracy at the LHC [22]. The observation of any deviation from these predictions would imply new physics beyond the Standard Model. As was already noted, and will be discussed further in Section 5, the expectations for deviations are small in typical BSM scenarios. It is thus one of the main goals for a future e^+e^- collider is to achieve O(1%) precision in the measurement of Higgs boson couplings. This goal has been demonstrated to be achievable at the ILC [2,3,7,10] for the running scenarios with a baseline of $\sqrt{s} = 500$ GeV, based on full detector simulations for most of the observables.

Thus we focus here on the prospects for the measurement of Higgs boson couplings at the 250 GeV stage of ILC assuming a total integrated luminosity of 2 ab^{-1}.

In this section we will first introduce the basic observables that are used to fit for Higgs boson couplings. We will also discuss the expected precisions of branching ratios, which can be determined free of any theory assumptions. To quote absolutely normalized couplings, we need to determine the Higgs boson width, and this requires a theory framework. We will discuss the width determination in the κ and EFT formalisms described in the previous section, emphasizing the major consequences of the change from $\sqrt{s} = 500$ GeV to 250 GeV and the new observables that play an important role in the EFT approach. Unless explicitly stated, all numbers shown in this section are for a total integrated luminosity of 2 ab^{-1} and for beam polarization sharing as introduced in Section 2.

4.1 Basic observables: σ, $\sigma \cdot BR$

The SM cross sections for the leading Higgs production processes in e^+e^- annihilation with $(P_e, P_p) = (-0.8, +0.3)$ polarized beams are shown in Fig. 3. The process $e^+e^- \to Zh$ attains its maximum cross section at $\sqrt{s} = 250$ GeV, providing about half a million Zh events from an integrated luminosity of 2 ab^{-1}. This allows the precise measurement of the inclusive cross section σ_{Zh}, using the recoil mass technique, and of the rates $\sigma_{Zh} \cdot BR$ for various decay modes. Up-to-date estimates for measurements of σ_{Zh} and $\sigma_{Zh} \cdot BR$ are given in the Appendix of [20]. Most notably, σ_{Zh} is measured to 1.0% for both $(-+)$ and $(+-)$ initial polarization states at $\sqrt{s} = 250$ GeV. An example of the recoil mass distribution in the $Z \to \mu^+\mu^-$ channel is given in Figure 4 (left).

With both σ_{Zh} and $\sigma_{Zh} \cdot BR$ measured, the absolute branching ratios can be determined independently of any fitting formula. Among the SM branching ratios, the best measured ones would be BR_{bb} and $BR_{\tau\tau}$, with accuracies of 0.89% and 1.4% respectively. If there are O(1%) or larger exotic decay modes, a first hint would

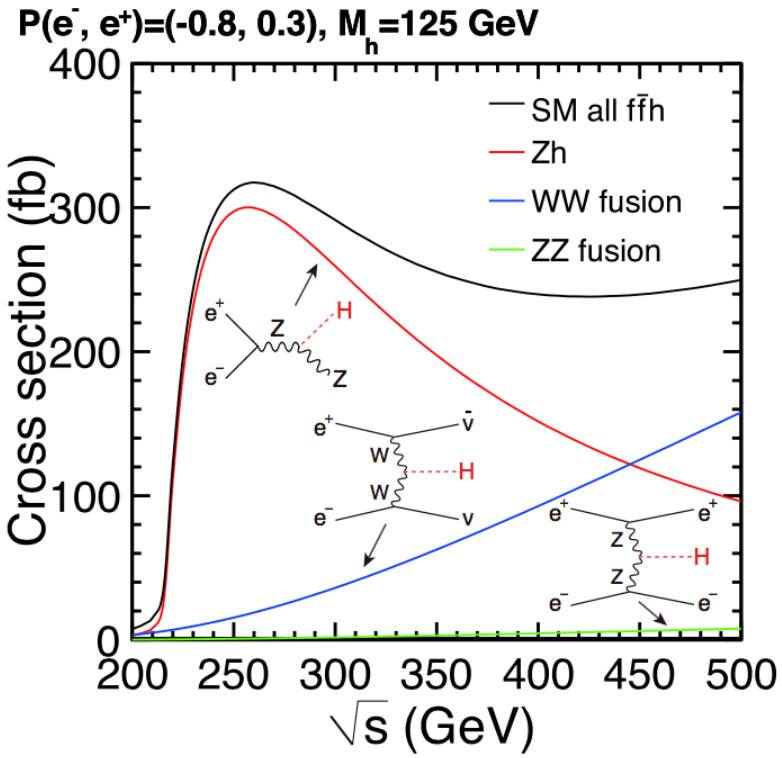

Figure 3: Cross sections for the three major Higgs production processes as a function of center of mass energy, from [2].

already be provided by observing the resulting deviations in BR_{bb} and $BR_{\tau\tau}$. The branching ratios BR_{cc} and BR_{gg}, which are very challenging to access directly at the LHC, can be measured to 3.2% and 2.7% respectively. BR_{WW} and BR_{ZZ}, which play a special role in the total width determination, can be measured to 1.9% and 6.7% respectively. The branching ratios to the rare decay modes, $BR_{\gamma\gamma}$ and $BR_{\mu\mu}$ are limited by available statistics and can be measured only to 13% and 27% respectively.[‡] However, these measurements can be improved by combination with LHC results, since the ratios of branching ratios $BR_{ZZ}/BR_{\gamma\gamma}$ and $BR_{\mu\mu}/BR_{\gamma\gamma}$ are expected to be measured at the HL-LHC, with accuracies of 2% and 12% [24, 25], respectively. The fact that h is produced in recoil against a Z boson gives sensitivity to invisible decay modes of the Higgs boson sufficient to provide a limit $BR_{inv} < 0.32\%$ at the 95% C.L. The sensitivity of the 250 GeV program to invisible and exotic Higgs decays will be discussed further in Section 6.

For the σ_{Zh} and BR measurements, there seems to be no problem in going from $\sqrt{s} = 500$ GeV to 250 GeV, despite the lower expected luminosity. In fact σ_{Zh} turns out to be better measured at 250 GeV, mainly thanks to the larger cross section and less significant beamstrahlung effect. On the other hand, the lowered energy is expected to have a significant impact on the measurement of the WW fusion process ($e^+e^- \to \nu\overline{\nu}h$), the cross section of which becomes almost a factor of 10 smaller. Moreover, due to the limited available phase space at 250 GeV, the missing mass spectrum in the $\nu\overline{\nu}h$ process is significantly overlapping with that in the $Zh, Z \to \nu\overline{\nu}$ process, as shown in Figure 4 (right). As a result, $\sigma_{\nu\nu h}\cdot BR_{bb}$ for the $(-+)$ polarization state can only be measured to 4.3%. There is a correlation of -34% with the $\sigma_{Zh}\cdot BR_{bb}$ measurement, which is needed to determine BR_{bb}. This has only a tiny effect on the final result.

4.2 Expected precisions for Higgs boson couplings in the κ formalism

Using only the basic observables introduced above, all of the Higgs boson couplings can be extracted via a global fit in the κ formalism defined above (2). The total width of the Higgs boson is given by

$$\Gamma_h = \frac{\Gamma_{ZZ}}{BR_{ZZ}} = \frac{\Gamma_{WW}}{BR_{WW}}, \tag{8}$$

where Γ_{ZZ} (Γ_{WW}) is the partial decay width to ZZ^* (WW^*). In the κ formalism, Γ_{ZZ} (Γ_{WW}) is determined via κ_Z (κ_W) from the measurement of σ_{Zh} ($\sigma_{\nu\nu h}$) based on a simple relation,

$$\Gamma_{ZZ} \propto \kappa_Z^2 \propto \sigma_{Zh} \quad (\Gamma_{WW} \propto \kappa_W^2 \propto \sigma_{\nu\nu h}). \tag{9}$$

[‡]A promising improvement to the $BR_{\mu\mu}$ estimate is presented in [23].

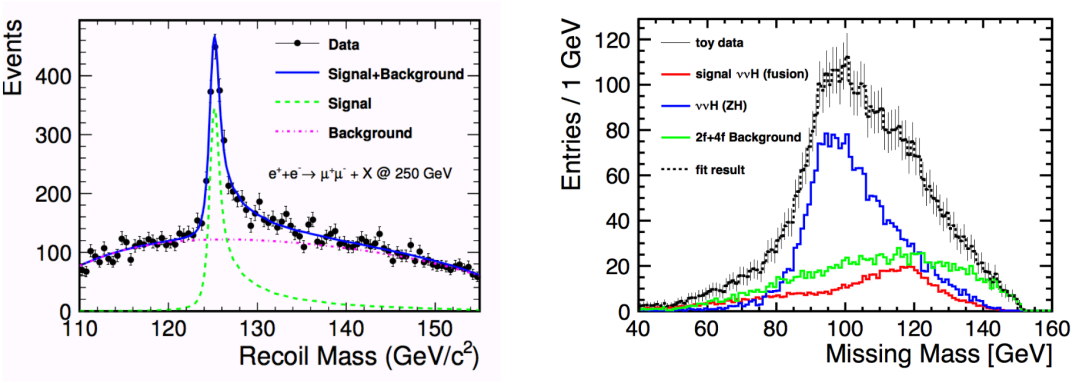

Figure 4: (left) recoil mass spectrum against $Z \to \mu^+\mu^-$ for signal $e^+e^- \to Zh$ and SM background at 250 GeV [26]; (right) missing mass spectrum for the signal $e^+e^- \to \nu\bar{\nu}h, h \to b\bar{b}$ and the SM background at 250 GeV [27, 28].

All the other couplings (κ_A) or partial decay widths (Γ_{AA}), e.g. $A = b, c, g, \tau, \mu, \gamma$, are then determined as

$$\kappa_A^2 \propto \Gamma_{AA} = \Gamma_h \cdot BR_{AA}. \tag{10}$$

As seen above, BR_{ZZ} is only measured to 6.7%, so if only the first half of (8) is used, all Higgs boson couplings (except κ_Z) would have an uncertainty greater than 3%. BR_{WW} is 10 times larger than BR_{ZZ} and so can be measured much more precisely. For this reason, it is well recognized that in the κ formalism the measurement of the WW fusion cross section $\sigma_{\nu\nu h}$ along with BR_{WW} (using the second half of (8)) is crucial for measurement of Γ_h and of all κ_A with $A \neq Z$. The expected precisions for Higgs boson couplings in the κ formalism are given in Table 1. We see that, at $\sqrt{s} = 250$ GeV, κ_Z is determined very precisely, with accuracy of 0.38%, but most other κ_A are determined to no better than $\sim 2\%$ (limited by $\sigma_{\nu\nu h}$ and BR_{ZZ} measurements). An exception is κ_γ, which is helped significantly by the fact that the fit makes use of the expected measurement of $BR_{ZZ}/BR_{\gamma\gamma}$ at the HL-LHC.

4.3 Expected precisions for Higgs boson couplings in the EFT formalism

In the EFT formalism, Higgs-Z interaction consists of two distinct Lorentz structures, shown in (4). As explained in the previous section, (9) is violated by the ζ_Z terms. Thus, the κ formalism is not model-independent, and it is not as general as the EFT formalism.

However, the EFT formalism allows Higgs boson couplings to be extracted via a much larger global fit. This fit includes not only the basic observables above but also additional observables of the reaction $e^+e^- \to Zh$, as well as observables of electroweak precision physics and $e^+e^- \to W^+W^-$. These latter measurements can

	ILC250		+ILC500	
	κ fit	EFT fit	κ fit	EFT fit
$g(hbb)$	1.8	1.1	0.60	0.58
$g(hcc)$	2.4	1.9	1.2	1.2
$g(hgg)$	2.2	1.7	0.97	0.95
$g(hWW)$	1.8	0.67	0.40	0.34
$g(h\tau\tau)$	1.9	1.2	0.80	0.74
$g(hZZ)$	0.38	0.68	0.30	0.35
$g(h\gamma\gamma)$	1.1	1.2	1.0	1.0
$g(h\mu\mu)$	5.6	5.6	5.1	5.1
$g(h\gamma Z)$	16	6.6	16	2.6
$g(hbb)/g(hWW)$	0.88	0.86	0.47	0.46
$g(h\tau\tau)/g(hWW)$	1.0	1.0	0.65	0.65
$g(hWW)/g(hZZ)$	1.7	0.07	0.26	0.05
Γ_h	3.9	2.5	1.7	1.6
$BR(h \to inv)$	0.32	0.32	0.29	0.29
$BR(h \to other)$	1.6	1.6	1.3	1.2

Table 1: Projected relative errors for Higgs boson couplings and other Higgs observables, in %, for fits in the κ and EFT formalisms. The ILC250 columns assume a total integrated luminosity of 2 ab^{-1} at $\sqrt{s} = 250$ GeV, shared by $(-+, +-, --, ++) = (45\%, 45\%, 5\%, 5\%)$ as described in Section 2. The ILC500 columns assume, in addition, a total integrated luminosity of 200 fb^{-1} at $\sqrt{s} = 350$ GeV, shared as $(45\%, 45\%, 5\%, 5\%)$, and a total integrated luminosity of 4 ab^{-1} at $\sqrt{s} = 500$ GeV, shared as $(40\%, 40\%, 10\%, 10\%)$. Three observables at the HL-LHC, $BR_{\gamma\gamma}/BR_{ZZ}$, $BR_{\gamma Z}/BR_{\gamma\gamma}$ and $BR_{\mu\mu}/BR_{\gamma\gamma}$, are included in all of the fits. The effective couplings $g(hWW)$ and $g(hZZ)$ are defined as proportional to the square root of the corresponding partial widths. The last two lines give 95% confidence upper limits on the exotic branching ratios. The detailed formulae used in the EFT fit, and the resulting covariance matrix, can be found in [16].

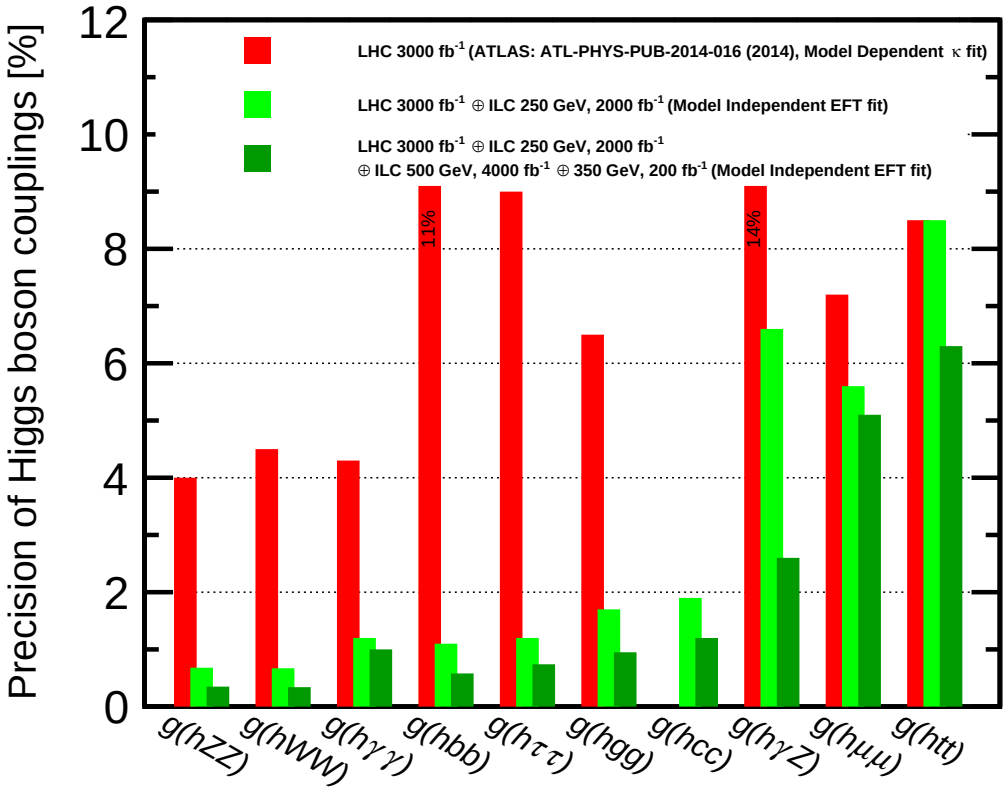

Figure 5: Illustration of the Higgs boson coupling uncertainties from fits in the EFT formalism, as presented in Table 1, and comparison of these projections to the results of model-dependent estimates for HL-LHC uncertainties presented by the ATLAS collaboration [24]. Earlier projections for HL-LHC are summarized in [29].

be included because the EFT Lagrangian is the complete Lagrangian and applies to all processes that occur in e^+e^- annihilation. Though the number of free parameters is significantly increased, it turns out that each parameter can be well controlled experimentally. Then the EFT improves significantly the measurement of Higgs boson couplings. The detailed strategy is explained in Section 3 and in [16, 20]. The results of Higgs boson coupling precisions based on the fitting program used in [16, 20] are given in Table 1. These results are illustrated and compared to the projections of Higgs coupling uncertainties at HL-LHC from the ATLAS experiment [24] in Fig. 5.

While the EFT coefficients parametrize shifts in the Higgs couplings from massive new particles, the fit that we use also allows Higgs decays to new particles lighter than $m_h/2$, manifested both as invisible Higgs decays and as other modes of exotic decay.[§] The small difference with the numbers in [20] comes from the different luminosity sharing among $(-+, +-, --, ++)$ assumed in the run plan presented in Section 2.

There are many interesting features in the Higgs boson coupling determination in the EFT formalism. It is worth emphasizing a few of them:

- A unique role is played by the inclusive Zh cross section, σ_{Zh}, enabled by the recoil mass technique. This remains the key element in the determination of the absolute normalization of all Higgs boson couplings. This freedom is mainly captured by the parameter c_H of the EFT formalism.

- The ratio of partial widths $\Gamma(h \to WW^*)/\Gamma(h \to ZZ^*)$ is determined very precisely, to $< 0.15\%$, mainly thanks to the constraints imposed on the EFT Lagrangian by $SU(2) \times U(1)$ gauge symmetry. In Table 1, we give values for effective couplings $g(hWW)$, $g(hZZ)$ defined to be proportional to the square roots of the partial widths. We see that $g(hWW)$ can be determined as precisely as $g(hZZ)$ without relying on the $\sigma_{\nu\nu h}$ measurement using the WW fusion process. This essentially solves the largest problem in measurement of Higgs boson couplings at $\sqrt{s} = 250$ GeV. Note that once $g(hWW)$ and $g(hZZ)$ are determined, Γ_h and all other couplings $g(hA\overline{A})$ are determined straightforwardly using (8) and (10).

- In $e^+e^- \to Zh$, new observables making use of both cross section and angular information are included. The information in these observables is contained in two parameters a_Z, b_Z for each initial polarization state [30]. The parameter a_Z contains the η_Z term and is essentially identical for the polarizations $e^-_L e^+_R$ and $e^-_R e^+_L$. The parameter b_Z contains ζ_Z or c_{WW} and also an effect of photon-Z mixing that is predicted by the EFT Lagrangian to depend on c_{WW} and related parameters. Estimates of the accuracy of the a_Z and b_Z measurements

[§]It is very conservative at an e^+e^- collider to allow that as many as 1% of Higgs decays will remain unrecognized as distinct processes. However, we do allow this for the purpose of this fit.

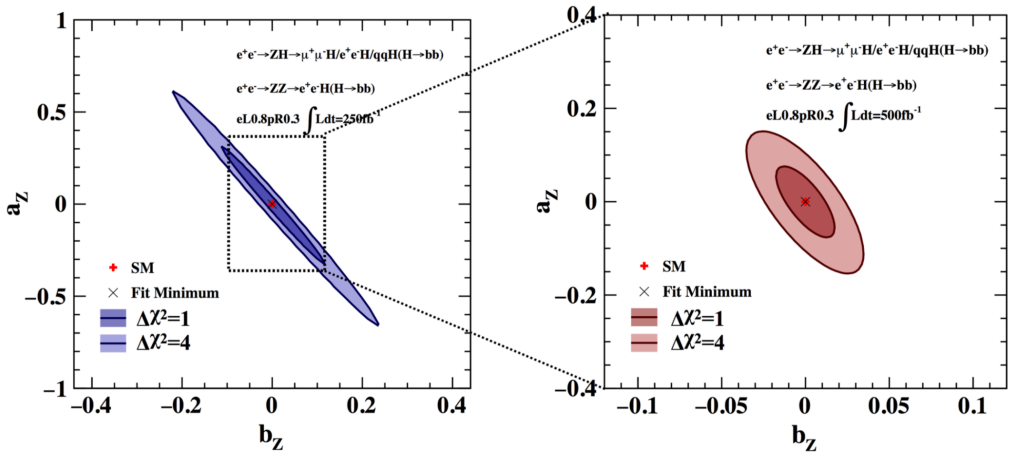

Figure 6: Contour plots for a_Z versus b_Z from [30]: for $\sqrt{s} = 250$ GeV with 250 fb^{-1} (left); for $\sqrt{s} = 500$ GeV with 500 fb^{-1} (right).

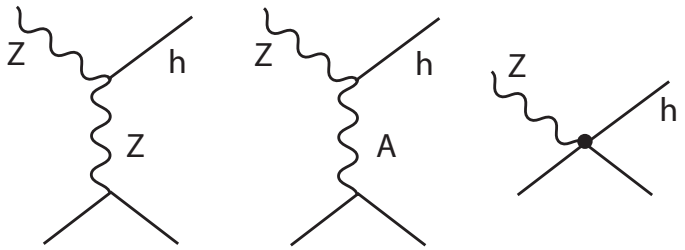

Figure 7: Feynman diagrams contributing to the amplitudes for $e^+e^- \to Zh$.

for individual polarization states, based on full detector simulation described in [30], are given in the Appendix of [20]. It is found that accuracies of the a_Z and b_Z determinations at 250 GeV are rather limited compared to that at 500 GeV; see Fig. 6. Luckily, there are other powerful means to help constrain c_{WW}.

- The photon-Z mixing effect that contributes to b_Z leads an additional diagram for $e^+e^- \to Zh$ with an s-channel photon instead of a Z. This diagram is shown in Fig. 7 along with a third diagram that arises from dimension-6 operator vertices. The interference between the first two diagrams is constructive for $e^-_L e^+_R$ and destructive for $e^-_R e^+_L$. Since the mixing effect depends strongly on c_{WW}, this EFT coefficient can be constrained very well using measurement of the polarization asymmetry in σ_{Zh}. Note that this polarization asymmetry in σ_{Zh} can be determined from using $\sigma_{Zh} \cdot BR$ measurements (which can be done with hadronic decay modes of the Z) as well as from inclusive cross section

measurements (which are dominated by leptonic decays of the Z). This allows more of the total data set to be used to constrain c_{WW}. The overall effect of beam polarizations on the determination of Higgs boson couplings can be found in Table 4 of [20].

- The decays $h \to \gamma\gamma$ and $h \to Z\gamma$ are loop-induced in the SM, but receive corrections at the tree level from dimension-6 operators. Thus, $\Gamma_{\gamma\gamma}$ and $\Gamma_{Z\gamma}$ are very sensitive to the operator coefficients c_{WW}, c_{WB} and c_{BB}, the same set of operators that determine ζ_A, ζ_{AZ}, ζ_Z and ζ_W. The measurements of $BR_{ZZ}/BR_{\gamma\gamma}$ and $BR_{\gamma Z}/BR_{\gamma\gamma}$ from the HL-LHC turn out to be very helpful, providing tight constraints on two linear combinations of c_{WW}, c_{WB} and c_{BB}, even though the projected accuracy for the $Z\gamma$ decay is only 31% [24]. It will be interesting to study whether any observable at ILC can measure the $hZ\gamma$ coupling directly to still better accuracy.

- The Triple Gauge Couplings (TGCs) measured in $e^+e^- \to W^+W^-$ play a very important role in fixing three of the 17 relevant EFT coefficients. So it is important that ILC will dramatically improve the measurement of TGCs over what has been accomplished at LEP2 and LHC. We will discuss this measurement in Section 8 below.

- The rightmost diagram in Figure 7 is induced by contact interactions from dimension-6 operator coefficients that correct the Z-lepton vertices measured from precision electroweak observables. These parameters appear in σ_{Zh} with very large coefficients, of order $2s/m_Z^2 \sim 15\,(60)$ at $\sqrt{s} = 250\,(500)$ GeV. It turns out that the constraints on these coefficients is improved over that from the current precision electroweak measurements by the comparison of Higgs cross sections at 250 and 500 GeV.[¶] Alternatively, the EFT fit would be assisted by improvement of precision electroweak measurements, either by direct e^+e^- running at the Z pole or by measurements of the polarization asymmetry of the radiative return process $e^+e^- \to Z\gamma$. This is another topic that needs further investigation.

4.4 Measurement of the Higgs boson mass and CP

The uncertainty in the Higgs boson mass (δm_h) is a source of systematic error for predictions of Higgs boson couplings. In most cases, $\delta m_h \sim 0.2\%$ would be already sufficient, but this is not true for $h \to ZZ^*$ or $h \to WW^*$. It has been pointed out in [31] that

$$\delta_W = 6.9 \cdot \delta m_h, \qquad \delta_Z = 7.7 \cdot \delta m_h, \tag{11}$$

[¶]The fit described here uses only the current uncertainties in precision electroweak measurements, except for an improvement in the uncertainty in Γ_W to 0.1% expected from ILC measurements of final states in $e^+e^- \to W^+W^-$.

where δ_W and δ_Z are the relative errors for $g(hWW)$ and $g(hZZ)$ respectively. At the 250 GeV ILC, the Higgs boson mass can be measured very precisely, with an accuracy of 14 MeV using the leptonic recoil channel as shown in Fig. 4 (left). This results in systematic errors for δ_W and δ_Z of 0.1%. The study of the new beam parameters discussed in Section 2, which would increase the beamstrahlung effect significantly, should pay attention to this issue.

At the 250 GeV ILC, Higgs CP properties can be probed via the $h\tau\tau$ coupling,

$$\Delta\mathcal{L}_{h\tau\tau} = -\frac{\kappa_\tau y_\tau}{\sqrt{2}} h\tau^+(\cos\phi + i\sin\phi\gamma_5)\tau^- \tag{12}$$

and the hVV coupling

$$\Delta\mathcal{L}_{hZZ} = \frac{1}{2}\frac{\tilde{b}}{v} hZ_{\mu\nu}\tilde{Z}^{\mu\nu}. \tag{13}$$

The CP phase ϕ in (12) can be measured with an accuracy of 3.8° [32], and $\tilde{b}$ in (13) can be measured with an accuracy of 0.5% [30]. The observation of even a small admixture of CP-odd coupling for the Higgs boson would indicate physics beyond the Standard Model, and might give a clue to the CP violation required in models of electroweak baryogenesis.

5 Comparison of the ILC capabilities for the Higgs boson to the predictions of new physics models

Now that we have presented the expectations for the accuracy of ILC measurements of the Higgs boson couplings, it is important to ask whether these expectations are strong enough to search for new physics beyond the reach of direct searches at the LHC. We will discuss that point in this section. First, we will survey models of new physics that affect the Higgs boson, review the diversity of models under consideration, and present the effects on the Higgs couplings predicted in the various types of models. Then we will present a representative sample of specific model points that demonstrate the power of the ILC measurements.

5.1 Models of electroweak symmetry breaking and the Higgs field

Our present understanding of the breaking of the $SU(2)\times U(1)$ gauge symmetry of the SM is crude and unsatisfactory. This point is, suprisingly, more easily grasped by condensed matter physicists than by particle physicists. Condensed matter physicists are familiar with the history of superconductivity, for which the basic understanding developed in two stages. In 1950, Landau and Ginzburg wrote a phenomenological theory of superconductivity that was, in fact, the model for the theory of the

Higgs field [33]. This model was successful and even predictive of many aspects of superconductivity, but, in this model, the basic fact of the phase transition to superconductivity was put in by hand. Only later, in 1957, did Bardeen, Cooper, and Schrieffer (BCS) create a fundamental theory of superconductivity based on pairing of electrons in a metal [34]. The BCS theory was not only a conceptual improvement but also predicted many new features of superconductivity that were beyond the reach of the Landau-Ginzburg description. In particle physics, we are now at the Landau-Ginzburg stage [35]. The difference from the condensed matter situation is that the interactions that drive electroweak symmetry breaking and lead to the phase transition must be new interactions, outside the SM, that have not yet been discovered. Thus, the exploration of the Higgs field offers the opportunity to discover genuinely new interactions of nature.

Many features of the SM argue that it cannot be a fundamental solution for electroweak symmetry breaking. For example, there are good reasons to believe that a scalar boson cannot be light (compared to Planck scale, for example) and give mass to all other particles in the SM without aid from other—as yet undiscovered—particles and interactions. These additional particles necessarily interact with the Higgs boson and can change the expectations for Higgs couplings to SM states.

Theories of physics beyond the SM are constructed to solve one or more outstanding problems that the SM does not address. They might attempt to explain the low mass of the Higgs boson without large fine-tunings as discussed above; they might posit dark matter candidates; they might explain the baryon asymmetry of the universe; they might unify the SM forces. In this space of theories there are many that can produce experimentally accessible non-SM signals to be discovered in the near term — some through direct searches of particles at the LHC's high-energy frontier, and others through a myriad of other experiments currently running or planned for the near future. Among these probes, though, precision measurement of the Higgs couplings is one of the most powerful. The reasons for this are two-fold. First, the Higgs sector is where we expect the most new interactions in many beyond the SM theories. Second, measurements in the Higgs sector have great room for improvement over current precision levels that can reveal new physics effects for beyond the SM theories that no other experiments could access.

Models that address the problems just listed can be constructed using many different approaches. A survey of these approaches, and estimates of the maximum possible effect on the Higgs boson couplings, was given in [36]. Table 2 lists three important classes of models and the corresponding estimates for maximal deviations in different couplings of the Higgs boson.

One class of models builds on the analogy with superconductivity. The order parameter for the Landau-Ginzburg potential of superconductivity turned out to be a composite state of electrons (Cooper pairs). It has been suggested that the Higgs

	$\Delta g(hVV)$	$\Delta g(ht\bar{t})$	$\Delta g(hb\bar{b})$
Composite Higgs	10%	tens of %	tens of %
Minimal Supersymmetry	$< 1\%$	3%	tens of %
Mixed-in Singlet	6%	6%	6%

Table 2: Estimated maximum deviations of Higgs couplings to various SM states allowed by three different scenarios of physics beyond the SM. The assumption is that no new physics associated with electroweak symmetry breaking is found at the HL-LHC ($3\,\mathrm{ab}^{-1}$ at $\sqrt{s} = 14\,\mathrm{TeV}$), and thus Higgs coupling measurements are the only potential signal for new physics. Adapted from [36].

boson state is also composite. If this is true, it has the potential to explain the large hierarchy between the Higgs mass and the Planck scale. A collection of some of the simplest approaches along this line leads to potentially large deviations of Higgs boson couplings to SM states compared to the expected measurement accuracies from the ILC.

A different class of models makes use of supersymmetry. Supersymmetry posits a symmetry between bosons and fermions that not only could explain the Higgs boson mass with respect to the Planck mass, but it could also be the source of dark matter, and it could be the key ingredient that enables the unification of forces at the high scale [37]. The symmetry requirements of supersymmetry require the introduction of two Higgs bosons – one that gives mass to up-type fermions and one that gives mass to down-type fermions. The two Higgs doublets mix and leave one CP-even eigenstate light, which is identified with the 125 GeV Higgs boson (h). It is straightforward to derive that this light boson h has couplings identical to those of the SM Higgs boson except for small deviations that are induced by mixings with the extra Higgs states and loop corrections involving the superpartners and the heavy Higgs bosons. These deviations of couplings can be well above 10% in the case of Higgs coupling to b quarks, even if no superpartner is ever found at the LHC in all its planned upgrade phases [36]. This is illustrated nicely by Fig. 8, where the authors scanned over hundreds of thousands of MSSM supersymmetric points [38]. They showed that many sets of parameters in the MSSM can never be found at the LHC but would be easily discernible through precision measurements at the ILC.

A third class of models postulates additional scalar fields. After all, there are many fermions, and there are many vector bosons. Multiple scalars are already required within supersymmetry, where in addition to scalar superpartners we stated that two Higgs bosons are required. But there are many more ideas of beyond the SM physics that incorporate several scalar bosons but do not cause ill effects elsewhere, by, for example, inducing too large flavor changing neutral currents. These multi-Higgs doublet models are classified as type I (in which one Higgs gives mass to fermions, and the other does not), type II (in which one Higgs gives mass to up fermions only

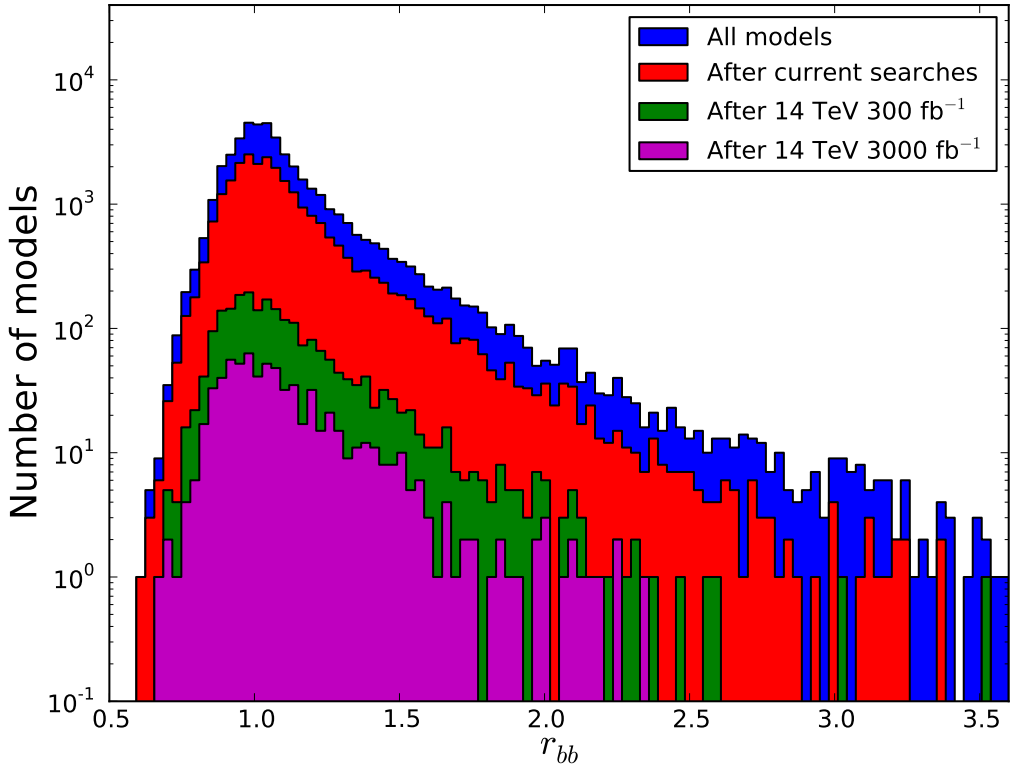

Figure 8: Histograms of the ratio $r_{bb} = \Gamma(h \to \bar{b}b)/\Gamma(h \to \bar{b}b)_{\rm SM}$ within a scan of the approximately 250,000 supersymmetry parameter sets after various stages of the LHC, assuming the LHC does not find direct evidence for supersymmetry. The purple histogram shows parameter points that would not be discovered at future upgrades of the LHC (14 TeV and 3 ab^{-1} integrated luminosity). From [38].

	Model	$b\bar{b}$	$c\bar{c}$	gg	WW	$\tau\tau$	ZZ	$\gamma\gamma$	$\mu\mu$
1	MSSM [38]	+4.8	-0.8	- 0.8	-0.2	+0.4	-0.5	+0.1	+0.3
2	Type II 2HD [39]	+10.1	-0.2	-0.2	0.0	+9.8	0.0	+0.1	+9.8
3	Type X 2HD [39]	-0.2	-0.2	-0.2	0.0	+7.8	0.0	0.0	+7.8
4	Type Y 2HD [39]	+10.1	-0.2	-0.2	0.0	-0.2	0.0	0.1	-0.2
5	Composite Higgs [40]	-6.4	-6.4	-6.4	-2.1	-6.4	-2.1	-2.1	-6.4
6	Little Higgs w. T-parity [41]	0.0	0.0	-6.1	-2.5	0.0	-2.5	-1.5	0.0
7	Little Higgs w. T-parity [42]	-7.8	-4.6	-3.5	-1.5	-7.8	-1.5	-1.0	-7.8
8	Higgs-Radion [43]	-1.5	- 1.5	+10.	-1.5	-1.5	-1.5	-1.0	-1.5
9	Higgs Singlet [44]	-3.5	-3.5	-3.5	-3.5	-3.5	-3.5	-3.5	-3.5

Table 3: Percent deviations from SM for Higgs boson couplings to SM states in various new physics models. These model points are unlikely to be discoverable at 14 TeV LHC through new particle searches even after the high luminosity era ($3\,\mathrm{ab}^{-1}$ of integrated luminosity). From [20].

and one to down fermions only), and type X and Y models (with more complicated discrete symmetries that protect flavor observables) [39].

5.2 Comparisons of models to the ILC potential

All of these ideas lead to models with deviations from the SM expectations of the couplings of the 125 GeV Higgs boson to SM states. Table 3 collects a set of models of new physics based on the ideas described in the previous section and on several additional ideas of interest to theorists. For each model, we chose a representative parameter point for which the predicted new particles would be beyond the reach of the 14 TeV LHC with the full projected data set. The deviations of Higgs couplings from the SM expectations at these representative model points are listed in the Table. (For details, see [20] as well as the papers cited in Table 3.) These examples illustrate diverse possibilities for models with significant deviations of the Higgs couplings from the SM expectation that would be allowed even if the LHC and other experiments are not able to discover the corresponding new physics beyond the SM. We should make clear that the quantitative statements to follow refer to these particular models at the specific parameter points shown in the Table. Figure 9 shows graphically the ability of ILC measurements to distinguish the Higgs boson couplings in the models in the Table from the SM expectations and from the expectations of other models. Each square shows relative goodness of fit for the two models in units of σ. The top figure is based on the covariance matrix from the 250 GeV stage of the ILC, corresponding to the second column of Table 1. The bottom figure reflects the full ILC program with 500 GeV running, corresponding to the fourth column of Table 1. It is noteworthy that, once it is known that the Higgs boson couplings deviate significantly from the

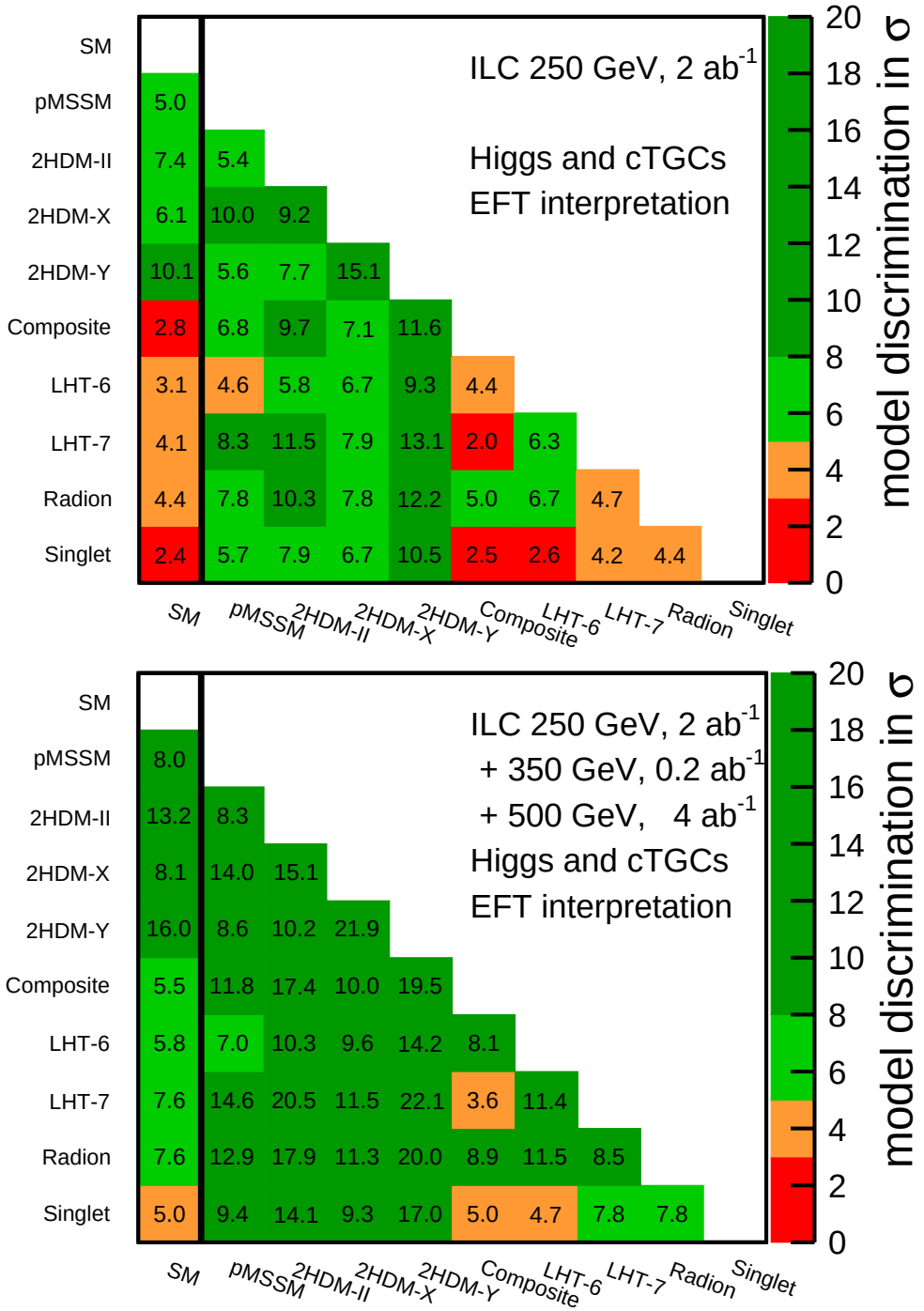

Figure 9: Graphical representation of the χ^2 separation of the Standard Model and the models 1–9 described in the text: (a) with 2 ab^{-1} of data at the ILC at 250 GeV; (b) with 2 ab^{-1} of data at the ILC at 250 GeV plus 4 ab^{-1} of data at the ILC at 500 GeV. Comparisons in orange have above 3 σ separation; comparison in green have above 5 σ separation; comparisons in dark green have above 8 σ separation. From [20], with slight modifications to account for the beam polarization scheme in Section 2.

SM predictions, the pattern of the deviations is characteristic for each model and distinguishable from the patterns predicted by other models in the set.

The evidence for significant deviations in the Higgs boson couplings would demonstrate that there is new physics beyond the SM that affects the Higgs field. The observation of the pattern of deviations would give us information on the properties of this new physics and point the way to further model-building and experimental exploration. This is a route to a deeper understanding of nature that the ILC offers us.

6 Invisible and exotic Higgs decays

In addition to the expected decays of the Higgs boson whose analysis was discussed in the previous two sections, the Higgs boson could also have additional decay modes that are not predicted by the SM. The ILC at 250 GeV will accumulate a data set containing half a million Higgs bosons tagged by recoiling Z bosons. This will provide an ideal environment to search for any possible final state of Higgs decay.

Exotic decays of the Higgs boson are expected in many theoretical models. An attractive way to model the dark matter of the universe is to assume the existence of a "hidden sector" consisting of one or more fields with no SM gauge charges. Since particles of a hidden sector do not couple through gauge forces, their interactions with SM particles are highly model-dependent and can be very feeble. Such particles can be consistent with all existing experimental constraints even if their masses are well below the weak scale. If some of the hidden-sector particles are stable, these could make up the observed dark matter. For example, in the "Strongly-Interacting Massive Particle" (SIMP) scenario [45, 46], dark matter consists of mesons produced by confinement of a QCD-like gauge group in the dark sector. A light hidden sector also appears in well-motivated theoretical models of electroweak symmetry breaking such as the "Twin Higgs" model [47]. Hidden-sector particles have also been invoked as an explanation of the apparent discrepancy between the experimental and theoretical values of the anomalous magnetic moment of the muon, and a number of other experimental anomalies. In light of this, there is strong interest in experimental searches for these particles, and a number of approaches are currently being pursued or studied [48, 49].

To connect the hidden-sector particles to initial states with Standard Model particles, it is necessary to add a term to the Lagrangian that connects these sectors. There are precisely three dimension-4 operators that can make this connection:

$$\epsilon\, B_{\mu\nu}\hat{F}^{\mu\nu}\ , \qquad \epsilon\, |\varphi|^2|\hat{S}|^2\ , \qquad \epsilon\, L^\dagger\cdot\varphi\hat{N}\ , \tag{14}$$

where $B_{\mu\nu}$ is the $U(1)$ field strength, φ is the Higgs doublet, and L is the lepton

doublet of the SM and fields with hats are in the hidden sector. These are called the "gauge portal", "Higgs portal", and "neutrino portal", respectively. Note that the neutrino portal also involves the Higgs field. Almost all of the attention in the reports [48, 49] is given to the gauge portal, which can be studied with low-energy fixed-target experiments, among other techniques. This leaves open a wealth of other possibilities, especially if the hidden sector particles have masses above a few GeV.

Decays of the Higgs boson offer a unique opportunity for very sensitive searches for a light hidden sector using the Higgs and neutrino portals. The SM Higgs width is tiny, $\Gamma_h/m_h \simeq 3 \cdot 10^{-5}$. Thus, the branching fraction of Higgs decays to hidden-sector states could be sizable even if its couplings to such states are rather small.

Signatures of Higgs decays into the hidden sector are model-dependent. One possibility is that the hidden-sector particles are stable or sufficiently long-lived that they do not decay inside the detector. Since interactions between hidden-sector particles and ordinary matter are extremely weak, they will escape the detector unseen, resulting in an "invisible Higgs decay" signature. Experiments at an electron-positron collider have excellent sensitivity to this signature, due to their ability to tag Higgs bosons using the recoil mass technique. The 250 GeV ILC is expected to be sensitive to invisible Higgs decays with branching ratios as small as 0.3% [20], a factor of 20 below the expected HL-LHC sensitivity.

Another interesting possibility is that the hidden-sector particles decay inside the detector. If the decay occurs purely within the hidden sector, such final states would remain invisible. On the other hand, if the decay products include SM particles[‖], they are potentially observable as "exotic" Higgs decay modes. A large variety of decay topologies and specific final states are possible; a systematic discussion can be found in the recent overviews of Higgs exotic decays [15, 50]. Two simple and theoretically well-motivated examples are:

1. $f\overline{f}+ \not{E}_T$, where f is an SM fermion. For example, in SUSY models with an extra gauge-singlet scalar s, such as the NMSSM, this final state arises from the decay chain $h \to \widetilde{\chi}_1^0\widetilde{\chi}_2^0$, $\widetilde{\chi}_2^0 \to s\widetilde{\chi}_1^0$, $s \to f\overline{f}$, with either on-shell or off-shell s. The flavor of f is dictated by the couplings of s to quarks and leptons, which are highly model-dependent. If the connection to the hidden sector is through the neutrino portal, the neutrino will provide missing energy even if the mediator fermion labelled $\hat{N}$ in (14) produces only visible final particles.

2. $(f\overline{f})(f'\overline{f}')$, where f and f' are SM fermions, and brackets indicate a resonant pair. These final states arise from a decay chain $h \to aa$, $a \to f\overline{f}$, where a is

[‖]Even if all couplings between the hidden sector and the SM are small, such decays may occur with significant probability, *e.g.* in cases when no competing decays within the hidden sector are kinematically available.

a gauge-singlet scalar particle, for example a composite of a confining hidden-sector gauge group in Twin Higgs models. Again, the fermion flavors involved in these decays are highly model-dependent.

Experiments at the (HL-)LHC will have excellent sensitivity to exotic Higgs decay modes to electrons, muons, or photons. However, final states involving quarks or tau leptons are very challenging at the LHC. The ILC at 250 GeV offers a perfect environment to search for such final states, due to low QCD backgrounds and Higgs tagging with recoil-mass technique. The paper [51] estimated the sensitivity of the 250 GeV ILC with 2 ab^{-1} integrated luminosity to the exotic decay topologies listed above. In the $f\bar{f}+\not{E}_T$ channels, with $f = j, b$ or τ, the ILC will be sensitive to branching ratios in the $10^{-4} - 10^{-3}$ range, *vs.* a projected sensitivity of at best 20% at the LHC. For the $(f\bar{f})(f'\bar{f}')$ topology, the improvement is equally dramatic: for example, branching ratios of the $(b\bar{b})(b\bar{b})$, $(c\bar{c})(c\bar{c})$, $(j\bar{j})(j\bar{j})$ channels will be probed down to the level of 10^{-3}, improving the LHC sensitivity by two orders of magnitude.

7 Opportunities for discovering direct production of new particles

Although the LHC experiments have carried out extensive searches for new particles, these searches have well-recognized limitations. The LHC exclusions are strongest for particles produced by QCD interactions and are less powerful for particles produced through electroweak processes, which have smaller cross sections. Discovery at the LHC is especially difficult if the new particles decay with very small visible energy, for example, if a charged particle decays to a stable neutral partner separated in mass by less than 15 GeV. For particles of this type, the best current limits can still come from the LEP 2 experiments.

It is not clear *a priori* that ILC at 250 GeV offers a significant discovery reach beyond LEP 2. The center-of-mass energy of 250 GeV is only about 40 GeV above the highest energies reached at LEP 2. This argument, however, overlooks three features of the ILC program. First, the ILC run at 250 GeV offers about 1000 times more integrated luminosity than collected at the highest energies by all 4 LEP experiments together ($\sim 250\,\text{pb}^{-1}$ per experiment in the year 2000 vs. $2\,\text{ab}^{-1}$). Second, the ILC offers polarized beams which, especially in the $(+-)$ configuration, can suppress SM backgrounds by 1-2 orders of magnitude, thereby increasing the sensitivity to rare BSM events. Finally, the ILC detectors will profit from 30 years of advances in technology, giving more than an order of magnitude better momentum and impact parameter resolutions, a factor 2 improvement in the jet energy scale, and considerably tightened hermeticity.

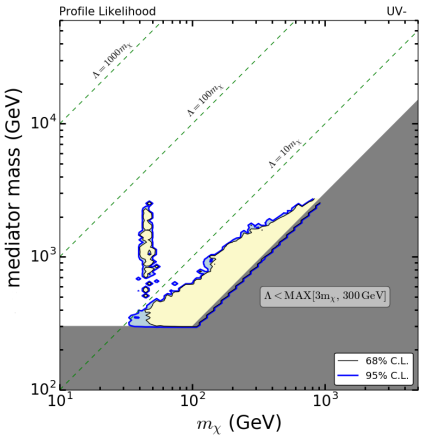

(a)

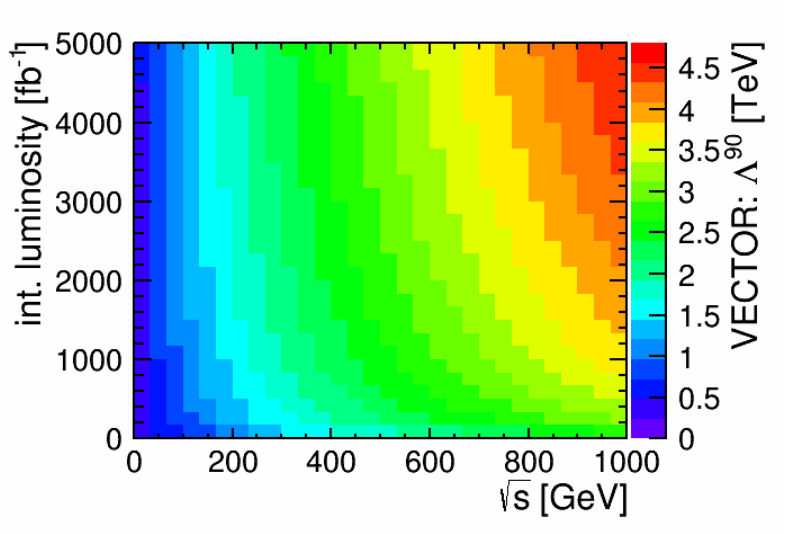

(b)

Figure 10: Sensitivity of WIMP searches in the mono-photon channel, from [56]: (a) The yellow area indicates regions in WIMP parameter space which are not probed by current or future direct detection experiments or by searches at the (HL-)LHC. (b) New physics scale Λ probed by mono-photon searches at the ILC as a function of center-of-mass energy and integrated luminosity.

Therefore, any search channel which was not kinematically but instead cross-section limited at LEP 2 offers significant discovery potential at the ILC, even at 250 GeV. One prominent example is the search for additional light Higgs bosons. Because the 125 GeV Higgs boson has couplings to W and Z close to those of the SM, additional bosons must have suppressed couplings to the Z boson. These can be searched for as at LEP in specific decays modes, but probing couplings to the Z boson at least one order of magnitude smaller. In addition, the much higher luminosity at the ILC will allow searches for such particles independently of their decay mode via the recoil technique [52].

Even some SUSY searches were not yet kinematically limited at LEP. For example, the LEP lower limit on the mass of the supersymmetric partner of the τ-lepton is only 26.3 GeV [53] in the general MSSM, *i.e.*, when allowing any mixing and any mass difference to the lightest SUSY particle.

Another interesting goal is the search for heavy sterile neutrinos. Improving the limits from LEP 1 on the mixing with the SM neutrinos at masses below 45 GeV would require an extended run at the Z pole. But such sterile neutrinos could also be produced directly together with a SM neutrino. This process would show up as an apparent deviation in the W^+W^- production cross-section [54, 55]. In this case, the sensitivity is expected to expand the regime probed by LEP 2 by at least an order of magnitude.

An important focus of new particle searches both at LHC and ILC is the search for WIMP pair production, which is observed at ILC in the mono-photon channel. This search was studied in full simulation at 500 GeV, and the results of this study have been extrapolated to lower center-of-mass energies [56]. The case of a singlet-like fermion WIMP is illustrated in Fig. 10a. Substantial regions of parameter space at masses below $\sim$ 120 GeV will remain even after a combined likelihood analysis including current and future direct detection as well as (HL-)LHC prospects. Figure 10b shows the new physics scale Λ which can be probed by the ILC for the case of a vector-like fermion WIMP and a vector-like operator dominating its interactions with SM particles, as a function of the center-of-mass energy and the integrated luminosity, assuming a sharing between different beam helicity configurations of (40%, 40%, 10%, 10%) as described in Section 2. For 2 ab^{-1} at 250 GeV, new physics scales up to 1.9 TeV can be probed.

8 $e^+e^- \to W^+W^-$ at 250 GeV

Measurements of the γW^+W^- and ZW^+W^- triple gauge boson couplings (TGC's) test the $SU(2) \times U(1)$ gauge boson self-coupling structure of the SM and probe BSM physics. As for the particle searches described in the previous section, the ILC at

250 GeV with 2 ab^{-1} offers substantial improvement beyond the results of LEP 2, which have not yet been surpassed by LHC.

The most general Lorentz invariant γW^+W^- or ZW^+W^- vertex contains 7 complex parameters, denoted by $g_1^V, g_4^V, g_5^V, \kappa_V, \lambda_V, \tilde{\kappa}_V, \tilde{\lambda}_V$, $V = \gamma, Z$ [57]. In total there are 14 complex parameters to consider. At tree-level, in the SM, $g_1^V = \kappa_V = 1$ and all other parameters are zero. SM radiative corrections are on the order of $2 \times 10^{-2} M_Z^2/s$ [58].

The primary focus of TGC studies is the search for modifications to the TGC's from BSM physics at energy scales well beyond the e^+e^- center-of-mass energy. As described in Section 3, such physics is parameterized by an effective Lagrangian with dimension-6 operators that respects $SU(2) \times U(1)$ gauge symmetry. CP-conserving and CP-violating effects are separately measurable, with comparable accuracy. Here we will concentrate on the CP-conserving operators. In this context, only six real TGC parameters are relevant: $g_1^V, \kappa_V, \lambda_V$ for $V = \gamma, Z$. Furthermore, three $SU(2) \times U(1)$ constraints

$$\begin{aligned} g_1^\gamma &= 1 \\ \kappa_Z &= -(\kappa_\gamma - 1)\tan^2\theta_W + g_1^Z \\ \lambda_Z &= \lambda_\gamma \end{aligned} \tag{15}$$

reduce the number of free parameters to three: $g_1^Z, \kappa_\gamma, \lambda_\gamma$.

TGC's are measured at the ILC through the processes $e^+e^- \to W^+W^-$, and $e^-\gamma \to \nu_e W^-$, where the initial state γ refers to either a virtual or beamstrahlung photon. Initial state beam polarization can be used to disentangle γW^+W^- couplings from ZW^+W^-. The W^- production polar angle Θ and the rest frame fermion polar and azimuthal angles, (θ^*, ϕ^*) and $(\overline{\theta}^*, \overline{\phi}^*)$, associated with the decays of the W^- and W^+, respectively, can be precisely measured. The correlated distributions of these five angles will be used as a polarization analyzer to separate out the multiple combinations of transversely and longitudinally polarized W^- and W^+ bosons.

In order to properly estimate the TGC sensitivity of the ILC at $\sqrt{s} = 250$ GeV, a full detector simulation study of signal and background processes including luminosity-weighted beam energy spectra and beam-beam background event overlay is required. Such an analysis is ongoing, but results are not yet available. For this report, we extrapolate full simulation ILC results at $\sqrt{s} = 500$ GeV [59] down to $\sqrt{s} = 250$ GeV in order to obtain the precision for three parameter fits. Since one parameter fits were not done in the ILC studies at $\sqrt{s} = 500$ GeV, we extrapolate LEP 2 one parameter fit results at $\sqrt{s} \approx 200$ GeV [60] up to $\sqrt{s} = 250$ GeV and use the minimum of this extrapolation and the three parameter result as estimates for the one parameter fits.

When extrapolating TGC statistical errors from one energy to another at least two effects must be considered [61]. Clearly a $1/\sqrt{\sigma L}$ statistical factor must be included

		total error ($\times 10^{-4}$)			correlation		
Exp	N_{par}	g_1^Z	κ_γ	λ_γ	g_1^Z κ_γ	g_1^Z λ_γ	κ_γ λ_γ
LEP 2	3	516	618	376	-0.17	-0.62	-0.15
ILC 250	3	4.4	5.7	4.2	0.63	0.48	0.35
LEP 2	1	300	626	292	–	–	–
LHC	1	319	1077	198	–	–	–
HL-LHC	1	19	160	4	–	–	–
ILC 250	1	3.7	5.7	3.7	–	–	–

Table 4: TGC precisions for LEP 2, Run1 at LHC, HL-LHC and the ILC at $\sqrt{s} = 250$ GeV with 2000 fb^{-1} luminosity (ILC 250). The LEP 2 result is from ALEPH [60] at $\sqrt{s} \approx 200$ GeV with 0.68 fb^{-1}. The LHC result is from ATLAS [62] at $\sqrt{s} = 7$ TeV with 4.6 fb^{-1}. The HL-LHC estimate is from a 2013 overview of HL-LHC physics [63].

where σ and L are the cross-section and integrated luminosity, respectively, at a particular center of mass energy. Furthermore, a factor inversely proportional to the center of mass energy squared, s, must be used to account for the energy dependence of the $SU(2) \times U(1)$ diagram cancellation. In total a factor k_{ex} is used to extrapolate TGC statistical error from energy A to energy B:

$$k_{ex} = \left(\frac{\sigma_A L_A}{\sigma_B L_B}\right)^{\frac{1}{2}} \left(\frac{s_A}{s_B}\right)^2 \quad . \tag{16}$$

We assume that systematic errors are scaled by the same factor k_{ex} as results are extrapolated from one energy to another.

The TGC precisions for the ILC at $\sqrt{s} = 250$ GeV with 2000 fb^{-1} luminosity (ILC 250) are shown in Table 4 and Figure 11, along with results from LEP 2, LHC, and HL-LHC. Results for one parameter fits where the other two anomalous couplings are set to zero are shown along with results for the full three parametrer fit.

At ILC 250 the three TGC's should be measured with accuracies ranging from $4 - 6 \times 10^{-4}$. Comparing the one parameter ILC 250 fit results with HL-LHC, the ILC 250 gives significantly better results for g_1^Z and κ_γ and roughly the same result for λ_γ.

The large sample of W^+W^- and single-W events at the ILC 250 also offers an excellent setting for the measurement of the W mass through kinematic reconstruction of W pair events and calorimetric comparison of hadronic W and Z decays. These strategies are described in [6, 64]. The systematics limit, which we estimate as 2.4 MeV, should already be reached at the 250 GeV stage of the ILC.

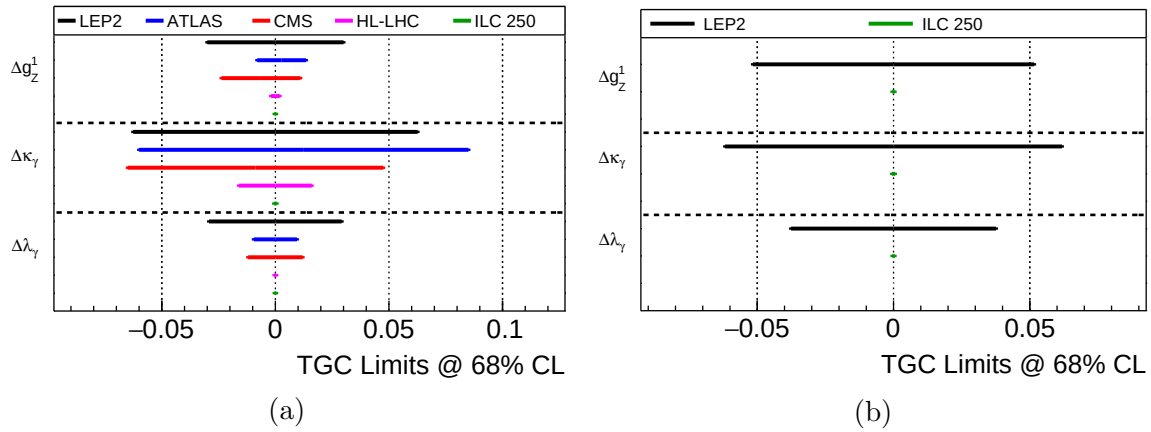

Figure 11: TGC precisions for LEP 2, Run1 at LHC, HL-LHC and the ILC at $\sqrt{s} = 250$ GeV with 2000 fb^{-1} luminosity (ILC 250) using one parameter fits (a) and for LEP 2 and ILC 250 using three parameter fits (b).

9 Two-fermion production at 250 GeV

At an e^+e^- collider, the processes $e^+e^- \to f\overline{f}$ can be measured with high precision for any SM fermion species. In the Z pole experiments at LEP and SLC, the measurement of two-fermion production in various final states gave what are still the best measurements of the weak mixing angle $\sin^2\theta_w$ [65]. At higher energies explored at LEP 2, interference of the s-channel photon and Z diagrams produces order-1 forward-backward and polarization asymmetries. These can be used to probe for new effects, beyond the SM, that would be seen in interference with the SM contributions. As for the physics topics presented in the previous two sections, the ILC at 250 GeV will lead to an improvement by more than an order of magnitude in the sensitivity to these effects, due to the higher energy, the dramatically larger luminosity, and the use of beam polarization.

New physics contributions to $e^+e^- \to f\overline{f}$ arise in a variety of models. One possible source is a Z' boson. The LEP 2 experiments placed lower limits on the masses of various types of Z' bosons in the range 500–800 GeV (and 1760 GeV for a sequential Z boson) [66]. The corresponding limits from the 250 GeV ILC would be of order 5 TeV, comparable to the reach of LHC direct searches. These limits would be improved by a factor 2 with ILC running at 500 GeV. The ILC searches are specific as to the flavor of the fermion species, the helicity of the coupling to electrons, and also, through the polarized forward-backward asymmetry, the helicity of the coupling to the final-state fermion.

Another possible source of corrections to the SM is the presence of extra dimensions, including the warped extra dimensions proposed in the model of Randall and

Sundrum [67] that also can be interpreted as a dual description of new strong interactions associated with the Higgs sector. Two-fermion processes, together with the Higgsstrahlung process [68], are a very powerful probe for these models. In these models, the new physics resonances called Kaluza-Klein excitations modify the electroweak couplings to fermions in a well-defined way. For example, in the model proposed in [69], only couplings to the (heavy) third generation quarks (t, b) are modified. On the other hand, the model proposed in [70] predicts modifications to the couplings of all charged fermions. In both cases, one expects effects of the order of about 10% already at a center-of-mass energy of 250 GeV.

An issue of particular interest is the measurement of the electroweak form factors of the b quark. The b_L is certainly a heavy quark in the sense of the previous paragraph, since it is in the same $SU(2) \times U(1)$ multiplet as the top quark. The b_R might or might not be affected by Higgs strong interactions. It is important to test for this possibility. There are some tantalizing hints for non-standard behavior of the b_R. There is a long-standing 3σ discrepancy between the value of $\sin^2\theta^\ell_w$ derived from the b forward-backward asymmetry at LEP and the value obtained at the SLC using polarized beams [65]. Non-standard effects in the form factors of the b_R might explain this discrepancy. Hints for new physics are coming from Heavy Flavour Physics, as described, for example, in [71]. In [72], it is argued that the anomalies can be accommodated by requiring different degrees of compositeness of fermions in a dual theory.

A recent full simulation study [73] has investigated the process $e^+e^- \to b\bar{b}$ at 250 GeV and for an integrated luminosity of 0.5 ab^{-1}, shared between the different beam polarizations. Figure 12 shows that, already for this initial phase, the ILC precision for the b quark form factors will be much improved compared to the LEP results on the Z pole, except for the case of the b_L vector coupling, which is strongly constrained from $BR(Z \to b\bar{b})$. A particularly interesting improvement is in the b_R vector coupling g_{RZ}, for which the ILC will outperform existing LEP results by about a factor of five. The measurements at the ILC will thus deliver the final word on the partial compositeness of the b_R, which is central to the open issues listed above.

Based on [73] and on earlier studies of the t quark [74], it seems to be feasible to extend these quark form factor measurements to the c quark. This study can take advantage of the running at 250 GeV, since the decay products of the corresponding bottom or charm mesons are less boosted than at $\sqrt{s} = 500$ GeV. This is beneficial for the assignment of tracks to secondary vertices.

Fermion pair production is a powerful tool to set limits on fermion compositeness and may be probed by effective four-fermion vertices. The paper [75] discusses the sensitivity of two-fermion production to new physics in terms of these contact interactions at CM energies of $\sqrt{s} = 500$ GeV and $\sqrt{s} = 800$ GeV. Extrapolating from this study, we estimate that the ILC at 250 GeV will produce limits on the Λ scale of

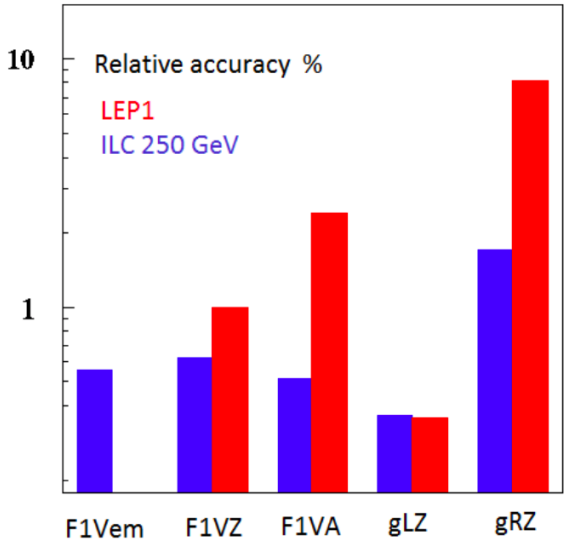

Figure 12: Comparisons of the precisions for the electroweak form factors of the b quark expected for the ILC at 250 GeV for 500 fb^{-1} with those obtained by LEP. The figure is taken from [73]

contact interactions (interpreted as the inverse of the radius of a composite fermion) at roughly 60 TeV.

10 Program of the ILC beyond 250 GeV

We have seen above that the 250 GeV ILC has a great potential to discover BSM physics through precision measurements of the Higgs boson and various other electroweak processes, thanks to its well-defined initial state, its clean environment without QCD backgrounds, and its powerful polarized beams. We have also seen that these virtues of the ILC would allow the discovery of new particles already at 250 GeV. Such a new particle could include a dark matter particle, or a new particle that couples only very weakly to the SM particles, or new particles with a compressed mass spectrum that makes their detection extremely difficult at the LHC.

The real advantage of the linear collider is, however, its upgradability to higher energies by either expanding the length of the linacs or exploiting more advanced acceleration technology that would be available by the time of the upgrade. In Section 2, we outlined a reference staging scenario that consists of operation of the ILC at three energy stages: 250, 350, and 500 GeV. The physics goals of the higher energy stages have already been described in the reports [7] and [8]. However, it is worth briefly recalling the main points here.

- The 350 GeV stage of the ILC will enable us to carry out an energy scan of the $t\bar{t}$ threshold. This set of measurements will allow us to determine the threshold value of the top quark mass $m_t(1S)$ to 50 MeV. (See Section 3.2 of [8].) This is not only an improvement in accuracy over the expectation for m_t at the LHC, but also it is a measurement of a different quantity that is better defined theoretically and more closely connected to the top quark mass relevant for weak decay processes and grand unification. The threshold top quark mass is closely related to the $\overline{MS}$ top quark mass; the conversion error is negligible if anticipated improvements in the value of $\alpha_s(m_Z)$ are realized. If no deviations from the SM predictions are seen in other processes, this measurement will definitively settle the issue of the vacuum stability of the SM [76].

- The 500 GeV stage of the ILC will provide a further improvement in the precision of the Higgs boson couplings accessible through Higgs decay by almost a factor 2 beyond the already strong results at 250 GeV. We have already demonstrated this in Table 1 and shown the implications for new physics discovery in Fig. 9.

- The 500 GeV stage of the ILC will give us access to two additional Higgs boson couplings that are not available at 250 GeV. The first of these is the Higgs coupling to $t\bar{t}$, which is measureable using the process $e^+e^- \to t\bar{t}h$. This Higgs boson coupling has large deviations from the SM expectation in many models in which the Higgs boson is composite or partially composite, for example [77]. The accuracy expected in this coupling with 500 GeV and 4 ab^{-1} of data is 6%. The limited accuracy is due to the fact that 500 GeV is very close to the $t\bar{t}h$ threshold. Comparable running at 550 GeV will enable an accuracy of 3%. At still higher energies, a 2% determination is possible [3]

- The 500 GeV stage of the ILC will also bring us above threshold for the process $e^+e^- \to Zhh$, from which it is possible to measure the triple Higgs coupling. This measurement will give a first glimpse of the Higgs field potential beyond the measurement of the Higgs mass. The measurement of the triple Higgs coupling is a crucial test for models of electroweak baryogenesis. In models of this type, the Higgs phase transition must be of first order, and so a large deviation from the SM expectation for the potential is required [78,79]. The expected accuracy of the ILC measurement will be 27%, sufficient to test this prediction.

  Analyses of the triple Higgs coupling measurement typically assume that the only non-Standard effect is the change in the triple Higgs coupling and ignore the other possible effects of new physics on the observables. In [16], these effects are studied within the EFT formalism and found to be potentially very substantial. It is shown there that high precision measurements on single-Higgs processes are required to unambiguously interpret measurements of double-Higgs production. At the ILC at 500 GeV, it is shown that the systematic error on the triple

Higgs coupling from other new physics effects is smaller than 5%, due to the high precision constraints that the ILC will give on the other 16 relevant EFT coefficients. There is no comparable strategy to address this point at hadron colliders. In pp collisions, many more EFT coefficients come into play, the constraints on these coefficients are weaker, and the dependence of the double Higgs production cross section on these coefficients is much stronger.

- The 500 GeV stage of the ILC will measure the form factors for the top quark couplings to the photon and Z individually to accuracies below 1%. Models of composite Higgs bosons usually also entail partially composite top quarks. This leads to substantial deviations from the SM expectations for the $Zt\bar{t}$ form factors, with characteristic differences between the couplings to t_L and t_R depending on the model. A compilation of model predictions is given in [7]. These measurements give an additional, independent, route to the discovery of new physics associated with new strong interactions in the Higgs sector.

- The 500 GeV stage of the ILC will improve the reach of searches for dark matter pair production, Higgsino production, and production of other challenging proposed particles beyond the expectations given in Section 7. The variety of new particles that can be discovered in direct production at 500 GeV is reviewed in [8].

- The 500 GeV stage of the ILC will substantially improve the discovery potential of the precision measurements of $e^+e^- \to W^+W^-$ and $e^+e^- \to f\overline{f}$ described in Sections 8 and 9. The reach in terms of new physics scales will increase by almost factor of 2.

We do not know the ultimate energy reach of the ILC technology. The ILC TDR documents a possible extention to 1 TeV based on current superconducting RF technology [11, 12]. However, the capabilities of superconducting RF accelerator are improving at a rapid pace; see, for example, [80]. Over a longer term, we can imagine the development of advanced high-gradient accelerator technologies that could enable an e^+e^- collider at 10 TeV or higher in the ILC tunnel [81]. If the 250 GeV ILC can discover the existence of new physics, later stages of the ILC Laboratory could explore this physics at its own natural energy scale. The 250 GeV ILC is not an endpoint; rather, it is the first step toward a new method for uncovering physics beyond the SM.

11 Conclusions

The physics capabilities of the ILC at 250 GeV are formidable.

As we have explained in this paper, this facility will provide high-precision measurements of the couplings of the Higgs boson. These coupling determinations will be model-independent and the values of the output couplings will be absolutely normalized. Neither feature is possible at the LHC. The precisions available at the 250 GeV stage of the ILC are close to 1% for the Higgs coupling to the b quark and below 1% for the Higgs couplings to the W and Z. We have demonstrated that this capability allows the discovery of new physics for a variety of interesting models for which the predicted particles are too heavy to be discovered at the LHC.

The ILC at 250 GeV also allows deep searches for exotic decays of the Higgs boson. Such decays are expected, in particular, in models in which dark matter is a part of a "hidden sector" with no couplings to Standard Model gauge bosons. This program of searching for dark matter using the Higgs is orthogonal to searches for hidden sector particles with fixed target beams, a subject of much recent interest, and it is no less important.

The ILC at 250 GeV will also carry out searches for pair production of dark matter particles and other particles with small energy deposition that are difficult to uncover at the LHC. Although the energy increase from LEP 2 is small, the integrated luminosity of the ILC will be larger by a factor of 1000, leading to greatly improved reach for many searches. This luminosity increase and improvements in detector technology will also allow us to greatly improve the precision of measurements in $e^+e^- \to W^+W^-$ and $e^+e^- \to f\overline{f}$ and perhaps to expose new physics in those processes.

All of these approaches, and more, will benefit from operation of the ILC at higher energies. The ILC at 250 GeV, beyond the power of its own experiments, will be the first step along that road.

It is urgent today in particle physics to uncover physics beyond the Standard Model by any route. The experiments discussed in this report give a number of strategies for searches for new physics that are distinct from those currently being pursued at the LHC and elsewhere. These strategies have great potential. But to exploit them, we must construct the next e^+e^- collider. The particle physics community should make it a priority to fund and construct this machine as quickly as possible.

ACKNOWLEDGEMENTS

We are grateful to many people with whom we have discussed this document. Special thanks go to Rick Gupta, Howard Haber, JoAnne Hewett, Ahmed Ismail, Hugh Montgomery, Francois Richard, Sabine Riemann, Heidi Rzehak, and Graham Wilson. We are grateful for financial support for our work from many agencies around

the world. TB and MEP were supported by the US Department of Energy under contract DE–AC02–76SF00515. TB, MB, CG, MH, RK, JL, and JR are supported by the Deutsche Forschungsgemeinschaft (DFG) through the Collaborative Research Centre SFB 676 Particles, Strings and the Early Universe, projects B1 and B11. CG is also supported by the European Commission through the Marie Curie Career Integration Grant 631962 and by the Helmholtz Association through its recruitment initiative. HK and SJ are supported by the National Research Foundation of Korea under grant 2015R1A4A1042542. KF and TO are supported by the Japan Society for the Promotion of Science (JSPS) under Grants-in-Aid for Science Research 16H02173 and 16H02176. JT is supported by the JSPS under Grant-in-Aid 15H02083. MP is supported by the U.S. National Science Foundation through grant PHY-1719877. RP is supported by the Quarks & Leptons programme of the French IN2P3.

A Projected ILC physics measurement uncertainties

In Table 5, we summarize the projections for the uncertainties in the measurements discussed in this report.

It is noteworthy that the improvements in the Higgs coupling analysis reviewed in this paper allow us to claim stronger results for precision coupling determinations than in our previous reports, despite the fact that the proposed running energies are lower. It is especially interesting to compare the projections given in this report with those given in our 2013 white paper [3] and provided to the P5 panel that formulated the US strategic plan for particle physics in 2014 [83]. This comparison is shown in Table 6. All entries refer to "model-independent" coupling determinations. However, since the earlier analyses were done in the κ formalism, their results are less model-independent than those presented in this report. The program that we have presented here, even for the first stage at 250 GeV, will fulfill the promises that we made in 2013.

References

[1] T. Behnke *et al.*, "The International Linear Collider Technical Design Report - Volume 1: Executive Summary," arXiv:1306.6327 [physics.acc-ph].

[2] H. Baer *et al.*, "The International Linear Collider Technical Design Report - Volume 2: Physics," arXiv:1306.6352 [hep-ph].

[3] D. M. Asner, *et al.*, "ILC Higgs White Paper," in the Proceedings of the APS DPF Community Summer Study (Snowmass 2013), arXiv:1310.0763 [hep-ph].

Topic	Parameter	250 GeV	250 + 500 GeV	units
Higgs	m_h	14	14	MeV
	$g(hb\bar{b})$	1.1	0.58	%
	$g(hc\bar{c})$	1.9	1.2	%
	$g(hgg)$	1.7	0.95	%
	$g(hWW)$	0.67	0.34	%
	$g(h\tau\tau)$	1.2	0.74	%
	$g(hZZ)$	0.68	0.35	%
	$g(h\gamma\gamma)$	1.2	1.0	%
	$g(h\mu\mu)$	5.6	5.1	%
	$g(h\gamma Z)$	6.6	2.6	%
	$g(ht\bar{t})$	-	6.3	%,
	$g(hhh)$	-	27	%
	Γ_{tot}	2.5	1.6	%
	Γ_{invis}	0.32	0.29	%, 95% CL
Top	m_t	-	50	MeV (m_t(1S))
	Γ_t	-	60	MeV
	g_L^γ	-	0.6	%
	g_R^γ	-	0.6	%
	g_L^Z	-	0.6	%
	g_R^Z	-	1.0	%
	Re F_2^γ	-	0.0014	absolute
	Re F_2^Z	-	0.0017	absolute
	Im F_2^γ	-	0.0014	absolute
	Im F_2^Z	-	0.0020	absolute
W	m_W	2.4 MeV	2.4	MeV
	g_1^Z	4.4×10^{-4}	1.1×10^{-4}	absolute
	κ_γ	5.7×10^{-4}	1.4×10^{-4}	absolute
	λ_γ	4.2×10^{-4}	1.4×10^{-4}	absolute
Dark Matter	EFT Λ: D5	1.9	3.0	TeV, 90% CL
	EFT Λ: D8	1.8	2.8	TeV, 90% CL

Table 5: Projected accuracies of measurements of Standard Model parameters for the 250 GeV stage of the ILC program and the complete program with 500 GeV running, as described in Section 2 of this report. The projected integrated luminosities are: 2 ab^{-1} at 250 GeV, adding, for the full program, 0.2 ab^{-1} at 350 GeV and 4 ab^{-1} at 500 GeV. Initial state polarizations are as given at the end of Section 2. Uncertainties are listed as 1σ errors (except where indicated), computed cumulatively at each stage of the program. These estimated errors include both statistical uncertainties and theoretical and experimental systematic uncertainties. Except where indicated, errors in percent (%) are fractional uncertainties relative to the Standard Model values. For dark matter, the effective field theory Λ parameters are defined in [82]. More specific information for each set of measurements is given in corresponding chapter of this report.

Parameter	Snowmass 2013 : ILC(500)	ILC(LumUp)	this report : 250 GeV	250+500 GeV	units
$g(hb\bar{b})$	1.6	0.7	1.1	0.58	%
$g(hc\bar{c})$	2.8	1.0	1.9	1.2	%
$g(hgg)$	2.3	0.9	1.7	0.95	%
$g(hWW)$	1.1	0.6	0.67	0.34	%
$g(h\tau\tau)$	2.3	0.9	1.2	0.74	%
$g(hZZ)$	1.0	0.5	0.68	0.35	%
$g(ht\bar{t})$	14	1.9	-	6.3	%
Γ_{tot}	4.9	2.3	2.5	1.6	%

Table 6: Projected accuracies of measurements of Higgs couplings presented in this report, compared to the projected accuracies presented in the "ILC Higgs White Paper" prepared for Snowmass 2013 [3], Table 6.1. The column ILC(500) refers to the baseline program presented in that report: 250 fb^{-1} at 250 GeV plus 500 fb^{-1} at 500 GeV. The column ILC(LumUp) refers to the upgrade discussed in that report, with a total of 1.15 ab^{-1} at 250 GeV, 1600 ab^{-1} at 500 GeV, and 2.5 ab^{-1} at 1000 GeV.

[4] D. Asner, *et al.*, "Top quark precision physics at the International Linear Collider," in the Proceedings of the APS DPF Community Summer Study (Snowmass 2013), arXiv:1307.8265 [hep-ex].

[5] H. Baer, *et al.*, "Physics Case for the ILC Project: Perspective from Beyond the Standard Model," in the Proceedings of the APS DPF Community Summer Study (Snowmass 2013), arXiv:1307.5248 [hep-ph].

[6] A. Freitas, *et al.* "Exploring Quantum Physics at the ILC," in the Proceedings of the APS DPF Community Summer Study (Snowmass 2013), arXiv:1307.3962 [hep-ph].

[7] K. Fujii *et al.*, "Physics Case for the International Linear Collider," arXiv:1506.05992 [hep-ex].

[8] K. Fujii *et al.*, "The Potential of the ILC for Discovering New Particles," arXiv:1702.05333 [hep-ph].

[9] L. Evans and S. Michizono [Linear Collider Collaboration], "International Linear Collider Machine Staging Report 2017", arXiv:1711.00568 [physics.acc-ph].

[10] T. Barklow, J. Brau, K. Fujii, J. Gao, J. List, N. Walker and K. Yokoya, "ILC Operating Scenarios," arXiv:1506.07830 [hep-ex].

[11] C. Adolphsen *et al.*, "The International Linear Collider Technical Design Report - Volume 3.I: Accelerator & in the Technical Design Phase," arXiv:1306.6353 [physics.acc-ph].

[12] C. Adolphsen *et al.*, "The International Linear Collider Technical Design Report - Volume 3.II: Accelerator Baseline Design," arXiv:1306.6328 [physics.acc-ph].

[13] T. Behnke *et al.*, "The International Linear Collider Technical Design Report - Volume 4: Detectors," arXiv:1306.6329 [physics.ins-det].

[14] K. Fujii *et al.*, "The role of positron polarization for the inital 250 GeV stage of the International Linear Collider," arXiv:1801.02840 [hep-ph].

[15] D. de Florian *et al.* [LHC Higgs Cross Section Working Group], "Handbook of LHC Higgs Cross Sections: 4. Deciphering the Nature of the Higgs Sector," arXiv:1610.07922 [hep-ph].

[16] T. Barklow, K. Fujii, S. Jung, M. E. Peskin and J. Tian, arXiv:1708.09079 [hep-ph].

[17] S. F. Ge, H. J. He and R. Q. Xiao, JHEP **1610**, 007 (2016) [arXiv:1603.03385 [hep-ph]].

[18] J. Ellis, P. Roloff, V. Sanz and T. You, JHEP **1705**, 096 (2017) [arXiv:1701.04804 [hep-ph]].

[19] G. Durieux, C. Grojean, J. Gu and K. Wang, JHEP **1709**, 014 (2017) [arXiv:1704.02333 [hep-ph]].

[20] T. Barklow, K. Fujii, S. Jung, R. Karl, J. List, T. Ogawa, M. E. Peskin and J. Tian, arXiv:1708.08912 [hep-ph].

[21] M. E. Peskin and T. Takeuchi, Phys. Rev. Lett. **65**, 964 (1990), Phys. Rev. D **46**, 381 (1992).

[22] G. Aad *et al.* [ATLAS and CMS Collaborations], Phys. Rev. Lett. **114**, 191803 (2015) [arXiv:1503.07589 [hep-ex]].

[23] S. Kawada, "Status of $h\mu^+\mu^-$ analysis", presentation at ILD Analysis and Software Meeting on May 24, 2017, https://agenda.linearcollider.org/event/7648/.

[24] ATLAS Collaboration, ATL-PHYS-PUB-2014-016 (2014).

[25] ATLAS Collaboration, ATL-PHYS-PUB-2014-006 (2014).

[26] J. Yan, S. Watanuki, K. Fujii, A. Ishikawa, D. Jeans, J. Strube, J. Tian and H. Yamamoto, Phys. Rev. D **94**, 113002 (2016) [arXiv:1604.07524 [hep-ex]].

[27] J. Tian, "Update of $e^+e^- \to \nu\nu h$ analysis", presentation at ILD Analysis and Software Meeting on July 19, 2017, https://agenda.linearcollider.org/event/7703/contributions/39487/attachments/31909/48179

[28] C. Duerig, K. Fujii, J. List and J. Tian, arXiv:1403.7734 [hep-ex].

[29] S. Dawson *et al.*, "Working Group Report: Higgs Boson," in the Proceedings of the APS DPF Community Summer Study (Snowmass 2013), arXiv:1310.8361 [hep-ex].

[30] T. Ogawa, "Study of sensitivity to anomalous HVV couplings at the ILC", presentation at the EPS Conference on High Energy Physics, Venice, July 5-12, 2017, https://indico.cern.ch/event/466934/contributions/2588482/

[31] L. G. Almeida, S. J. Lee, S. Pokorski and J. D. Wells, Phys. Rev. D **89**, 033006 (2014) [arXiv:1311.6721 [hep-ph]].

[32] D. Jeans, "CP Measurements in $h \to \tau^+\tau^-$ at the ILC", presentation at the International Workshop on Linear Colliders (LCWS 2016) on December 4-9, 2016, https://agenda.linearcollider.org/event/7371/contributions/37895/.

[33] V. L. Ginzburg and L. D. Landau, Zh. Eksp. Teor. Fiz. **20**, 1064 (1950).

[34] J. Bardeen, L. N. Cooper and J. R. Schrieffer, Phys. Rev. **108**, 1175 (1957).

[35] J. D. Wells, Studies Hist. Phil. Sci. B (online 8 June 2017) https://doi.org/10.1016/j.shpsb.2017.05.004.

[36] R. S. Gupta, H. Rzehak and J. D. Wells, Phys. Rev. D **86**, 095001 (2012) [arXiv:1206.3560 [hep-ph]]; and, "Higgs boson coupling to b quarks: targets in the MSSM," MCTP-17-18 (2017).

[37] S. P. Martin, Adv. Ser. Direct. High Energy Phys. **21**, 1 (2010) [Adv. Ser. Direct. High Energy Phys. **18**, 1 (1998)] [hep-ph/9709356].

[38] M. Cahill-Rowley, J. Hewett, A. Ismail and T. Rizzo, arXiv:1308.0297 [hep-ph].

[39] S. Kanemura, H. Yokoya and Y. J. Zheng, Nucl. Phys. B **886**, 524 (2014) [arXiv:1404.5835 [hep-ph]].

[40] R. Contino, L. Da Rold and A. Pomarol, Phys. Rev. D **75**, 055014 (2007) [hep-ph/0612048].

[41] J. Hubisz, P. Meade, A. Noble and M. Perelstein, JHEP **0601**, 135 (2006) [hep-ph/0506042].

[42] C. R. Chen, K. Tobe and C.-P. Yuan, Phys. Lett. B **640**, 263 (2006) [hep-ph/0602211].

[43] J. L. Hewett and T. G. Rizzo, JHEP **0308**, 028 (2003) [hep-ph/0202155].

[44] S. Di Vita, C. Grojean, G. Panico, M. Riembau and T. Vantalon, JHEP **1709**, 069 (2017) [arXiv:1704.01953 [hep-ph]].

[45] Y. Hochberg, E. Kuflik, T. Volansky and J. G. Wacker, Phys. Rev. Lett. **113**, 171301 (2014) [arXiv:1402.5143 [hep-ph]].

[46] Y. Hochberg, E. Kuflik, H. Murayama, T. Volansky and J. G. Wacker, Phys. Rev. Lett. **115**, 021301 (2015) [arXiv:1411.3727 [hep-ph]].

[47] Z. Chacko, H. S. Goh and R. Harnik, Phys. Rev. Lett. **96**, 231802 (2006) [hep-ph/0506256].

[48] J. Alexander *et al.*, arXiv:1608.08632 [hep-ph].

[49] M. Battaglieri *et al.*, arXiv:1707.04591 [hep-ph].

[50] D. Curtin *et al.*, Phys. Rev. D **90**, 075004 (2014) [arXiv:1312.4992 [hep-ph]].

[51] Z. Liu, L. T. Wang and H. Zhang, Chin. Phys. C **41**, 063102 (2017) [arXiv:1612.09284 [hep-ph]].

[52] J. Yan, K. Fujii and J. Tian, arXiv:1601.06481 [hep-ph].

[53] J. Abdallah *et al.* [DELPHI Collaboration], Eur. Phys. J. C **31**, 421 (2003) [hep-ex/0311019].

[54] S. Antusch, E. Cazzato and O. Fischer, Int. J. Mod. Phys. A **32**, no. 14, 1750078 (2017) [arXiv:1612.02728 [hep-ph]].

[55] W. Liao and X. H. Wu, arXiv:1710.09266 [hep-ph].

[56] M. Habermehl, K. Fujii, J. List, S. Matsumoto and T. Tanabe, PoS ICHEP **2016**, 155 (2016) [arXiv:1702.05377 [hep-ex]].

[57] K. Hagiwara, R. D. Peccei, D. Zeppenfeld and K. Hikasa, Nucl. Phys. B **282**, 253 (1987).

[58] A. Arhrib, J. L. Kneur and G. Moultaka, [hep-ph/9603268].

[59] I. Marchesini, DESY-THESIS-2011-044.

[60] S. Schael *et al.* [ALEPH Collaboration], Phys. Lett. B **614**, 7 (2005).

[61] R. Karl, "Prospects for electroweak precision measurements and triple gauge couplings at a staged ILC", presentation at the EPS Conference on High Energy Physics 2017, Venice, https://indico.cern.ch/event/466934/contributions/2589875/.

[62] G. Aad *et al.* [ATLAS Collaboration], JHEP **1501**, 049 (2015) [arXiv:1410.7238 [hep-ex]].

[63] K. Moenig, "ATLAS & CMS physics prospects for the high-luminosity LHC", presentation at CLIC Workshop 2013, CERN, https://cds.cern.ch/record/1510150/files/ATL-PHYS-SLIDE-2013-042.pdf.

[64] G. W. Wilson, PoS ICHEP **2016**, 688 (2016).

[65] S. Schael *et al.* [ALEPH and DELPHI and L3 and OPAL and SLD Collaborations and LEP Electroweak Working Group and SLD Electroweak Group and SLD Heavy Flavour Group], Phys. Rept. **427**, 257 (2006) [hep-ex/0509008].

[66] S. Schael *et al.* [ALEPH and DELPHI and L3 and OPAL and LEP Electroweak Collaborations], Phys. Rept. **532**, 119 (2013) [arXiv:1302.3415 [hep-ex]].

[67] L. Randall and R. Sundrum, Phys. Rev. Lett. **83**, 3370 (1999) [hep-ph/9905221].

[68] A. Angelescu, G. Moreau and F. Richard, Phys. Rev. D **96**, no. 1, 015019 (2017) [arXiv:1702.03984 [hep-ph]].

[69] A. Djouadi, G. Moreau and F. Richard, Nucl. Phys. B **773**, 43 (2007) [hep-ph/0610173].

[70] S. Funatsu, H. Hatanaka, Y. Hosotani and Y. Orikasa, arXiv:1705.05282 [hep-ph].

[71] M. Neubert, "Heavy Flavour Physics", http://moriond.in2p3.fr/QCD/2017/MondayMorning/Neubert.pdf

[72] E. Megias, M. Quiros and L. Salas, JHEP **1707**, 102 (2017) [arXiv:1703.06019 [hep-ph]].

[73] S. Bilokin, R. Pöschl and F. Richard, arXiv:1709.04289 [hep-ex].

[74] M. S. Amjad *et al.*, Eur. Phys. J. C **75**, 512 (2015) [arXiv:1505.06020 [hep-ex]].

[75] J. A. Aguilar-Saavedra *et al.* [ECFA/DESY LC Physics Working Group], hep-ph/0106315.

[76] D. Buttazzo, G. Degrassi, P. P. Giardino, G. F. Giudice, F. Sala, A. Salvio and A. Strumia, JHEP **1312**, 089 (2013) [arXiv:1307.3536 [hep-ph]].

[77] R. Malm, M. Neubert and C. Schmell, JHEP **1502**, 008 (2015) [arXiv:1408.4456 [hep-ph]].

[78] A. Noble and M. Perelstein, Phys. Rev. D **78**, 063518 (2008) [arXiv:0711.3018 [hep-ph]].

[79] D. E. Morrissey and M. J. Ramsey-Musolf, New J. Phys. **14**, 125003 (2012) [arXiv:1206.2942 [hep-ph]].

[80] A. Grassellino *et al.*, Supercond. Sci. Technol. **30**, 094004 (2017) [arXiv:1701.06077 [physics.acc-ph]].

[81] J. P. Delahaye, E. Adli, S. Gessner, M. Hogan, T. Raubenheimer, W. An, C. Joshi and W. Mori, IPAC-2014-THPRI013.

[82] J. Goodman, M. Ibe, A. Rajaraman, W. Shepherd, T. M. P. Tait and H. B. Yu, Phys. Rev. D **82**, 116010 (2010) [arXiv:1008.1783 [hep-ph]].

[83] S. Ritz, *et al.*, *Building for Discovery: Strategic Plan for U.S. Particle Physics in the Global Context*, https://science.energy.gov/hep/hepap/reports/.